Structures and Aggregation of the MethylamineBorane Molecules, MenH3nN·BH3 (n = 13), Studied by X-ray Diffraction, Gas-Phase Electron Diffraction, and Quantum Chemical Calculations

Cite as:
Aldridge, S., Downs, A. J., Tang, C. Y., Parsons, S., Clarke, M. C., Johnstone, R. D. L., Robertson, H. E., Rankin, D. W. H., & Wann, D. A. (2009). Structures and Aggregation of the Methylamine−Borane Molecules, MenH3−nN·BH3 (n = 1−3), Studied by X-ray Diffraction, Gas-Phase Electron Diffraction, and Quantum Chemical Calculations. *Journal of the American Chemical Society*, 131(6), 2231-2243.

Manuscript received: 25/09/2008; Article published: 26/01/2009

Structures and Aggregation of the Methylamine−Borane Molecules, $Me_nH_{3-n}N{\cdot}BH_3$ (n = 1−3), Studied by X-ray Diffraction, Gas-Phase Electron Diffraction, and Quantum Chemical Calculations**

Simon Aldridge,[1] Anthony J. Downs,[1,*] Christina Y. Tang,[1] Simon Parsons,[2,*] Michael C. Clarke,[2] Russell D. L. Johnstone,[2] Heather E. Robertson,[2] David W. H. Rankin[2,*] and Derek A. Wann[2]

[1]Inorganic Chemistry Laboratory, University of Oxford, South Parks Road, Oxford OX1 3QR, UK.

[2]EaStCHEM, School of Chemistry, Joseph Black Building, University of Edinburgh, West Mains Road, Edinburgh, EH9 3JJ, UK.

[*]Corresponding authors; A.J.D.e-mail: tony.downs@chem.ox.ac.uk; S.P. e-mail: s.parsons@ed.ac.uk; D.W.H.R. e-mail: d.w.h.rankin@ed.ac.uk

[**]We thank the EPSRC for funding the electron-diffraction research (grant EP/C513649) and for post-doctoral funding of CYT (grant EP/F01600X). We are grateful also to Prof. Angelo Gavezzotti for a copy of the program OPiX for the PIXEL calculations.

Supporting information:
Details of the GED experiments; interatomic distances, refined and calculated amplitudes of vibration and perpendicular corrections for the SARACEN-restrained GED structures of 1 and 2; least-squares correlation matrices for the refined GED structures of 1 and 2; GED and calculated coordinates for 1 + its dissociation products and for 2; CIF files for the crystal structures of 1-3. Molecular scattering intensity and difference curves for the GED refinements of 1 + its dissociation products and of 2 (Figures S1 and S2). This material is available free of charge via the Internet at http://pubs.acs.org

Graphical abstract:

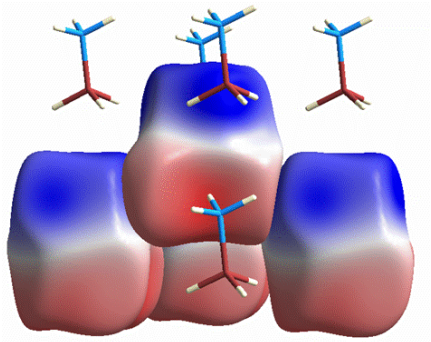

Abstract

The structures of the molecules methylamine-borane, $MeH_2N{\cdot}BH_3$, and dimethylamine-borane, $Me_2HN{\cdot}BH_3$, have been investigated by gas-phase electron diffraction (GED) and quantum chemical calculations. The crystal structures have also been determined for methylamine-, dimethylamine-, and trimethylamine-borane, $Me_nH_{3-n}N{\cdot}BH_3$ (n = 1-3); these are noteworthy for what they reveal about the intermolecular interactions and, particularly, the N–H···H–B dihydrogen bonding in the cases where n = 1 or 2. Hence structures are now known for all the members of the ammonia- and amine-borane series $Me_nH_{3-n}N{\cdot}BH_3$ (n = 0-3) in both the gas and solid phases. The structural variations and energetics of formation of the gaseous adducts are discussed in relation to the basicity of the $Me_nH_{3-n}N$ fragment. The relative importance of secondary interactions in the solid adducts with n = 0-3 has been assessed by the Semi-Classical Density Sums (SCDS-PIXEL) approach.

1. Introduction

The compound with the formal composition H_3NBH_3 has a long history[1-8] originating in the classic pioneering studies of Stock.[1] First identified as a product of the reaction between ammonia and diborane, it may be prepared, depending on the conditions, in two quite distinct forms, *viz*. (*i*) a simple molecular adduct ammonia-borane, $H_3N{\cdot}BH_3$, and (*ii*) a salt-like complex, the so-called 'diammoniate of diborane', $[(H_3N)_2BH_2]^+[BH_4]^-$. Ammonia-borane is a colorless solid that is stable at room temperature. The molecular nature of the compound is confirmed by analysis of the microwave spectrum of its vapor[9] and by X-ray[10] and neutron[11] diffraction studies of the crystalline solid. Crystallization results not only in a marked shrinkage of the B–N bond [from r_s = 1.6576(16) Å[9] to r = 1.564(6) Å[10]], but also in the development of short N–H···H–B intermolecular contacts (2.02 Å), affording one of the earliest examples of unconventional 'dihydrogen' bonds[12] to be recognized. This interaction between hydridic B–H and protic N–H bonds, prefiguring the potential for dihydrogen elimination, has also been signaled by Raman studies,[13] and investigated extensively through quantum chemical calculations[12,14,15] at varying levels of sophistication. These generally focus on the isolated dimer $[H_3N{\cdot}BH_3]_2$ or discrete oligomers[12,14] as models which do not resemble the crystal structure all that closely. Only Morrison and Siddick[15] have tackled the problem by using a periodic quantum mechanical approach with the full crystallographic unit cell as the model for calculation.

Replacing the hydrogen atoms of the ammonia fragment by methyl substituents gives in the methylamine-boranes $Me_nH_{3-n}N{\cdot}BH_3$ a series of molecular adducts. Every member for n = 1-3 resembles ammonia-borane in being a colorless solid at room temperature and has been well characterized, mainly in research carried out in the period 1935-1965;[2,3,6-8] only in the case of methylamine-borane has a salt-like form $[(MeH_2N)_2BH_2]^+[BH_4]^-$ also been described.[16] The only structure to be reported to date, however, is that of gaseous trimethylamine-borane, $Me_3N{\cdot}BH_3$, as determined from its gas-phase electron diffraction pattern[17] and

microwave spectrum;[18] this features a B–N coordinate link measuring 1.656(2) Å (r_g),[17] very similar to that in gaseous $H_3N{\cdot}BH_3$. Experimental estimates of the dissociation energies, D_e, for the reaction (1) reveal a steady increase with successive replacement of

$$Me_nH_{3-n}N{\cdot}BH_3(g) \longrightarrow Me_nH_{3-n}N(g) + BH_3(g) \qquad (1)$$

N–H by N–Me bonds (130, 146, 152, and 160 kJ mol^{-1} for n = 0, 1, 2, and 3, respectively).[19] This pattern parallels the proton affinity of the base,[20] and the values are more or less well reproduced by theoretical calculations.[21] Although no crystal structures have been reported hitherto for the methylamine-boranes $Me_nH_{3-n}N{\cdot}BH_3$ (n = 1-3), vapor pressure measurements have been made over a range of temperatures;[2,3,22] intriguingly, the enthalpies of vaporization they yield are significantly higher for $MeH_2N{\cdot}BH_3$ and $Me_2HN{\cdot}BH_3$ (79 and 77 kJ mol^{-1}) than for $Me_3N{\cdot}BH_3$ (57 kJ mol^{-1}), a pattern that runs counter to the polarizabilities of the molecules, if not to their dipole moments which appear to decrease with successive replacement of N–H by N–Me bonds.[3,9,18,23]

The coexistence of both hydridic B–H and protic N–H bonds in ammonia-borane and the methylamine-boranes $MeH_2N{\cdot}BH_3$ and $Me_2HN{\cdot}BH_3$, allied to a relatively strong B–N coordinate link, causes dihydrogen loss, as in eq 2, to be favored over dissociation in

$$Me_nH_{3-n}N{\cdot}BH_3 \longrightarrow 1/m\ [MeNBH]_m + (3-n)\ H_2 \qquad (2)$$

accordance with eq 1 under most conditions. When heated, or subjected to acid hydrolysis, these compounds do indeed release dihydrogen gas, but at a rate and with co-products that depend markedly on the precise conditions. Nevertheless, the combination of low molecular weight and high gravimetric hydrogen capacity (19.6, 11.2, and 6.8 wt% for $H_3N{\cdot}BH_3$, $MeH_2N{\cdot}BH_3$, and $Me_2HN{\cdot}BH_3$, respectively) has attracted intense interest in them as vehicles for chemical hydrogen storage.[7,8,24]

In the interests of having the fullest knowledge of the compounds so as better to understand their chemistry, we have determined the crystal structure of each of the three methylamine-boranes $Me_nH_{3-n}N{\cdot}BH_3$ (n = 1-3). In addition, we have determined the structures of the gaseous molecules $MeH_2N{\cdot}BH_3$ and $Me_2HN{\cdot}BH_3$ by gas-phase electron diffraction (GED) measurements and quantum chemical calculations. Hence the effects of methyl substitution have been investigated with regard to the structures and energetics of dissociation in molecules of the kind $Me_nH_{3-n}N{\cdot}BH_3$. Particular interest attaches not only to the structural changes that occur in the molecules on crystallization, but also, and more importantly, to the influence of intermolecular forces on the properties of the solid. To this end, the newly developed Semi-Classical Density Sums (SCDS-Pixel) approach, which considers molecules rather than individual atoms,[25] has been applied to the crystal structures of all four compounds in the series $Me_nH_{3-n}N{\cdot}BH_3$ for n = 0-3.

2. Experimental and Computational Section

Preparation of samples

The compounds $[MeNH_3]Cl$, $[Me_2NH_2]Cl$, $[Me_3NH]Cl$, and $LiBH_4$ (all from Aldrich, stated purities 99+, 99, 98, and 95%, respectively) were purified by recrystallization, the hydrochlorides from anhydrous ethanol and the tetrahydroborate from dry Et_2O. The adducts $MeH_2N{\cdot}BH_3$, **1**, $Me_2HN{\cdot}BH_3$, **2**, and $Me_3N{\cdot}BH_3$, **3**, were all prepared by essentially the same method involving the reaction of the relevant hydrochloride with $LiBH_4$, both freshly recrystallized, in dry Et_2O. The procedure was generally similar to that described elsewhere for the preparation of $Me_3N{\cdot}BH_3$ [26] and $Me_3N{\cdot}GaH_3$.[27] It involved adding the hydrochloride powder gradually to a stirred ethereal solution containing an equimolar quantity of $LiBH_4$ at –78 ºC over a period of *ca.* 30 min. Stirring of the reaction mixture continued for a further 30 min before the mixture was allowed to warm up to room temperature. Under these conditions, stirring was maintained for a further 5 h in order to ensure completion of the reaction. Thereafter, the mixture was cooled to –45 ºC and the ether removed under vacuum. The white powder remaining was heated *in vacuo* to temperatures ranging from 80 ºC, through 65 ºC, to 50 ºC to give a sublimate of **1**, **2**, and **3**, respectively. The purity of each product was checked by reference to its Raman spectrum and to the ^1H and ^{11}B NMR spectra of a tetrahydrofuran-d_8 solution.[2-4] Yields ranged from 70% for $MeH_2N{\cdot}BH_3$ to 78% for $Me_3N{\cdot}BH_3$ in relation to the quantities of the reagents taken and reaction 3.

$$LiBH_4 + [Me_nNH_{4-n}]Cl \longrightarrow Me_nH_{3-n}N{\cdot}BH_3 + LiCl + H_2 \qquad (3)$$

Gas-phase Electron Diffraction

Electron scattering intensities were measured for the vapors of **1** and **2** using the Edinburgh GED apparatus.[28] An accelerating voltage of 40 kV was used, resulting in an electron wavelength of approximately 0.06Å. The intensities were recorded on Kodak Electron Image films at two nozzle-to-film distances to maximize the scattering angle over which data were collected. Although there exists a port that allows data to be collected at a shorter nozzle-to-film distance, suitable vapor pressures were not attainable below the decomposition temperature. In order to obtain suitable vapor pressures, and to prevent condensation in the nozzle, the sample and nozzle were heated to the temperatures listed in Table S1.

The photographic films were scanned using an Epson Expression 1680 Pro flatbed scanner as part of a method that is now used routinely in Edinburgh and described elsewhere.[29] Data-reduction and least-squares refinement processes were carried out using the ed@ed program[30] employing the scattering factors of Ross *et al*.[31] The weighting points for the off-diagonal weight matrices, correlation parameters, and scale factors are given in Table S1.

X-ray Diffraction

Crystals of **1**, **2**, and **3** were each grown from an Et_2O solution kept at 0-4 ºC over a period of days. Single crystals were each mounted under perfluoropolyether oil on a glass fiber and cooled rapidly to 150 K. X-Ray diffraction data [λ(Mo Kα) = 0.710 73 Å] were then collected on an Enraf-Nonius Kappa CCD diffractometer. Table 1 gives the crystal data and other information relating to the structure determination and refinement for **1-3**. Crystal structures were solved by direct methods using SIR92[32] and refined using CRYSTALS.[33] Hydrogen atoms were located in difference maps and refined subject to restraints. Structures were visualized using DIAMOND[34] and MERCURY,[35] and miscellaneous geometry calculations were carried out using PLATON.[36]

Table 1. Crystallographic Data for Compounds **1**, **2**, and **3**

param	**1**	**2**	**3**
empirical formula	CH_8BN	$C_2H_{10}BN$	$C_3H_{12}BN$
fw	44.89	58.92	72.95
cryst dimens (mm)	0.40 × 0.20 × 0.04	0.50 × 0.20 × 0.05	0.50 × 0.30 × 0.20
cryst system	orthorhombic	monoclinic	rhombohedral
space group	*Pnma*	$P\,2_1/c$	$R3m$
unit cell dimens			
a (Å)	11.1350(8)	7.0452(6)	9.0792(5)
b (Å)	6.5575(4)	5.8368(5)	9.0792(5)
c (Å)	4.9194(3)	12.2335(14)	5.8922(5)
α (deg)	90	90	90
β (deg)	90	104.648(4)	90
γ (deg)	90	90	120
V (Å^3)	359.20(4)	486.71(8)	420.63(5)
Z	4	4	3
d(calcd) (Mg m^{-3})	0.830	0.804	0.864
abs coeff (mm^{-1})	0.048	0.046	0.049
θ_{max} (deg)	31.987	27.504	27.463
reflns measd	1813	2185	599
unique reflns (R_{int})	663 (0.037)	1104 (0.034)	130 (0.024)
no. of params	38	77	24
conventional R [R > 4σ(F)]	0.0381	0.0416	0.0283
weighted R (F^2 and all data)	0.1054	0.1120	0.0738
GOF on F^2 (S)	1.0019	1.0032	1.0092
largest diff. peak/hole (e Å^{-3})	+0.23/–0.11	+0.11/–0.11	+0.10/–0.10

Computational methods

Properties of the isolated molecules. All calculations were performed using the resources of the NSCCS[37] and the EaStCHEM Research Computing Facility[38] running the Gaussian 03 suite of programs.[39] For each of the molecules of **1** and **2**, a single minimum was identified on the potential-energy surface representing a C_s-symmetric structure. With the symmetry fixed, geometries were optimized, first at the spin-restricted Hartree-Fock level of theory with the 3-21G* basis set[40] on all atoms followed by the 6-31G* basis set[41] and then using MP2[42] to include the energy due to electron correlation. At this level the 6-311G* and 6-311++G** basis sets[43] were also used. The MP2 calculations included all electrons in the valence shell. Force constants calculated at the RHF/6-31G* level were subsequently employed, along with the program SHRINK,[44] to obtain initial amplitudes of vibration, and third derivatives of the energy (giving cubic anharmonicity terms) were then employed to give curvilinear perpendicular distance correction terms for the GED refinement. Thus, the structures obtained from the refinements are of the type $r_{a3,1}$. For a full discussion of the a3,1 nomenclature see reference 45.

Properties of the crystalline solids. Lattice and intermolecular interaction energies were evaluated for compounds in the series $Me_nH_{3-n}N{\cdot}BH_3$, with n = 0-3, by means of the Semi-Classical Density Sums (SCDS-PIXEL) method.[25,46] The geometry of each molecule was taken from the relevant crystal structure, the N–H and B–H distances we have determined by X-ray diffraction being extended to standard neutron lengths.[47] Without optimizing the geometry, an electron density map was then calculated on a three-dimensional grid with a step size of 0.08 Å for the molecule at the MP2/6-31G** level using Gaussian 03.[39] The pixels were then 'condensed' into super-pixels with dimensions 0.24 × 0.24 × 0.24 Å to expedite subsequent calculations (this is referred to as 'condensation level 3').[25b,46] The next stage of the calculations was to generate a cluster of molecules about a central reference molecule extending to 14 Å, as the basis for the intermolecular energy calculations. In order to determine the accuracy of the PIXEL procedure for boron compounds, calculations were also carried out on the following compounds for which both crystal structures and experimental sublimation energies are available (the CSD refcodes for the structural data are given in brackets:[48] B_2F_4 (unpublished crystal structure data), Me_2NBF_2 (DMABDF), pyridine-BBr_3 (BUNGEW), BPh_3 (TPHBOR), $B_3N_3H_3Cl_3$ (FUYTEY), and $B_3H_{12}N_3$ (FUZPAR). Sublimation energies were taken from the compilation by Chickos and Acree.[22c]

How these calculations proceeded can be illustrated using the Coulombic energy term. Intermolecular Coulombic energies in the cluster were calculated as sums of pixel-pixel, pixel-nucleus, and nucleus-nucleus terms, each pixel and each atomic nucleus having its own charge. Each interaction was evaluated on the basis of the standard electrostatic potential energy expression for two charges q_1 and q_2 separated by a distance r, *i.e.* eq 4:

$$E_{\mathrm{Coul}} = \frac{q_1 q_2}{4\pi\varepsilon_o r} \qquad (4)$$

Pixel-by-pixel summations of the polarization, dispersion, and repulsion energies were calculated *via* an analogous procedure, although this required the introduction of a total of four empirical parameters that had been previously optimized to reproduce experimental sublimation enthalpies for a range of organic molecular crystals.[25b] It should be explained here that the repulsion term corresponds to what is often referred to as 'Born' repulsion, that is, a quantum mechanical effect arising from overlap of charge clouds; ordinary electrostatic repulsion is part of the Coulombic term. Tests have shown that PIXEL results on organic systems compare well with the results of intermolecular perturbation theory and DFT calculations.[25b,49]

The PIXEL calculations yielded a total lattice energy derived from the sum of four components, namely, the electrostatic or Coulombic, polarization, dispersion, and repulsion terms, a correction being needed for structures in polar space groups.[50] Individual intermolecular contact energies were also calculated; in common with all the other energies, these are broken down into the four components already listed. This dissection into physically meaningful component terms is particularly valuable in any analysis of intermolecular interactions in the crystalline phase. However, it is important to recognize that PIXEL treats interactions at a *molecular* and not at an atomic level, and one must beware of falling into the trap of attributing a particular contact energy to a single prominent interatomic interaction, such as a hydrogen bond.

Calculation of Hirshfeld surfaces and associated electrostatic potentials was accomplished using CrystalExplorer.[51]

3. Results and Discussion

3.1. The isolated molecules: calculations and GED results

3.1(a) Calculations. The geometries of the molecules $Me_nH_{3-n}N{\cdot}BH_3$ (n = 0–3) were calculated using a variety of basis sets. As shown in Table 2, the B–N distances in the methylamine-boranes are very similar, while that in $H_3N{\cdot}BH_3$ is slightly longer. The most notable finding, however, was the basis-set dependence of the B–N distances. At the same level of theory, the use of augmented correlation-consistent quadruple-zeta basis sets shortens these bonds by around 0.015 Å compared with the use of a large Pople-style basis set. In all cases, the staggered conformation is the only minimum.

Table 2. Selected Calculated Parameters for $Me_nH_{3-n}N{\cdot}BH_3$ (n = 0–3).[a]

	B–N			<N–B–H	ΣB	ΣN
	MP2(full)/ 6-311++G**	MP2(full)/ aug-cc-pVTZ	MP2(full)/ aug-cc-pVQZ	MP2(full)/ 6-311++G**	MP2(full)/ 6-311++G**	MP2(full)/ 6-311++G**
Me_3NBH_3	1.638	—	1.624[b]	105.2	139.9	327.6
Me_2HNBH_3	1.633	1.623	1.619	104.8/105.3	340.2	326.8
MeH_2NBH_3	1.639	1.628	1.624	104.9/105.2	340.7	325.7
H_3NBH_3	1.653	1.645	1.639	104.8	341.1	323.4

[a] Distances are in Å; angles are in degrees.

[b] This value has been estimated on the basis that the MP2(full)/aug-cc-pVQZ value is consistently shorter than the MP2(full)/6-311++G** value by 0.014(1) Å.

3.1(b) GED Studies: Structures of the Gaseous Molecules $MeH_2N{\cdot}BH_3$, 1, and $Me_2HN{\cdot}BH_3$, 2.

Determining the structure of gaseous **1** was initially hampered by its propensity to dissociate partially at the temperatures required to obtain a suitably high vapor pressure. Despite collecting sets of data that matched well with one another, their fits to a model allowing for only $MeH_2N{\cdot}BH_3$ to be present in the vapor were poor. Specifically, the area in the radial-distribution curve where one would expect the B–N bond to appear showed a peak of greatly reduced area. Several models for dissociation and rearrangement were considered, including fitting the data to MeH_2N, $MeHNBH_2$ and cyclic-$[MeHNBH_2]_3$. However, none of these gave a satisfactory fit and, in the case of MeH_2N, the complete absence of a B···N contact proved to be a wrong assumption. In fact, the data suggested that $MeH_2N{\cdot}BH_3$ dissociates partially according to equation 5:

$$MeH_2N{\bullet}BH_3\ (g) \rightleftharpoons MeH_2N\ (g) + 1/2\ B_2H_6\ (g) \qquad (5)$$

The evidence for the presence of B_2H_6 rather than BH_3 is minimal, as one might expect when the scattering intensity is dependent on the atomic numbers of the atom pairs. However, when B_2H_6 was included in the model, a slightly improved fit was obtained in the region of the radial-distribution curve where the B···B interaction would be expected. In reality, it is possible that both "BH_3" and B_2H_6 are present, although "BH_3" has not, to our knowledge, been detected under conditions such as these. It was noted, in any case, that the precise identity of this dissociation moiety did not greatly affect the structures determined for either $MeH_2N{\cdot}BH_3$ or MeH_2N.

The model that was used in the refinement therefore described the structures of $MeH_2N{\cdot}BH_3$, MeH_2N and B_2H_6. To simplify matters, and guided by the results from high-level *ab initio* calculations, the parameters describing the amino group in **1** were also used to describe MeH_2N, with the modification described below.

Both **1** and MeH_2N were modeled with C_s symmetry and B_2H_6 with D_{2h} symmetry. The set of parameters used in the model is listed in Table 3; the atom numbering used to define **1** is shown in Figure 1(a).

As all the C–H bond lengths in **1** (and MeH_2N) were calculated to be very similar, a mean value was employed in the model (p_1). As the N–H distances are related through symmetry, only a single value was refined (p_2), and a mean value was again used for *r*B–H (p_3), here describing only those distances in **1**. Additional parameters were used to describe the B–H distances in B_2H_6 ($p_{16–17}$). A single C–N distance was described in the model, and a fixed difference applied to ensure that the C–N distance in MeH_2N is 0.015 Å shorter than that in **1**, as suggested by the *ab initio* calculations. The four angle parameters describing the positions of the amino and methyl hydrogen atoms ($p_{6–9}$) were applied identically to both **1** and MeH_2N. Three additional parameters were required to describe the borane group in **1** ($p_{10–12}$). A dummy atom, X, lying at the midpoint of the amino H···H vector was used to define X–N–C and X–N–B angles in **1** ($p_{13–14}$). Two angles were needed to complete the description of B_2H_6, one to describe the B–H–B angle of the bridging hydrogens and another for the H–B–H angle of the terminal hydrogens. Finally, a non-geometric parameter was used in the model to define the proportion of **1** that remained intact (*i.e.* did not dissociate).

(a)

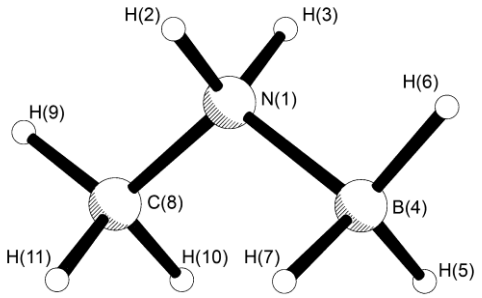

(b)

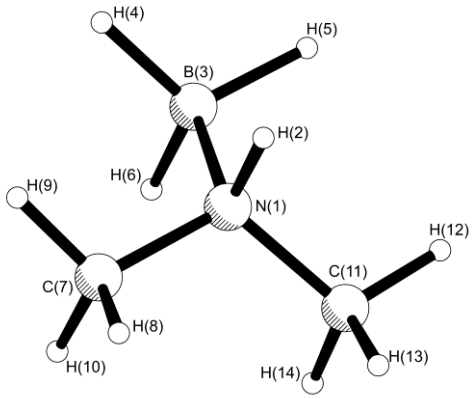

Figure 1. Molecular structure, including numbering scheme used in the GED studies (a) of $MeH_2N{\cdot}BH_3$, **1**, and (b) of $Me_2HN{\cdot}BH_3$, **2**.

Table 3. Refined ($r_{a3,1}$) and Calculated (r_e) Geometric Parameters for $MeH_2N{\cdot}BH_3$, **1**, and its Dissociation Products according to Equation 5 from the GED Study.[a,b]

	param	$r_{a3,1}$	r_e	restraint
Independent				
p_1	*r*C–H mean	1.112(7)	1.083	0.01
p_2	*r*N–H	1.025(10)	1.012	0.01
p_3	*r*B–H mean	1.208(10)	1.205	0.01
p_4	*r*C–N	1.449(3)	1.468	—
p_5	*r*N–B	1.602(7)	1.624	—
p_6	∠H–N–H	106.4(11)	106.4	1.0
p_7	∠N–C–H average	109.5(7)	109.9	1.0
p_8	∠N–C–H difference	3.9(6)	3.8	0.5
p_9	∠H–C–H	110.0(11)	110.2	1.0
p_{10}	∠N–B–H average	103.9(9)	105.3	1.0
p_{11}	∠H–B–H difference	0.5(5)	0.5	0.5
p_{12}	∠H–B–H	113.5(11)	113.5	1.0
p_{13}	∠X–N–C[c]	125.9(8)	124.8	1.0
p_{14}	∠X–N–B[c]	122.7(8)	121.8	1.0
p_{15}	∠B–H–B bridging	94.0(9)	85.6	1.0
p_{16}	*r*B–H bridging	1.329(10)	1.316	0.01
p_{17}	*r*B–H terminal	1.188(11)	1.180	0.01
p_{18}	∠H–B–H terminal	122.4(11)	122.4	1.0
p_{19}	proportion of molecules intact	0.67[d]	—	—
Dependent				
p_{20}	∠N–C–H(9)	111.4(7)	111.8	—
p_{21}	∠N–C–H(10)	107.6(7)	108.0	—
p_{22}	∠N–B–H(5)	103.6(10)	105.0	—
p_{23}	∠N–B–H(6)	104.2(9)	105.5	—
p_{24}	∠B–N–C	111.4(5)	113.4	—

[a] Refers to an MP2(full)/aug-cc-pVQZ calculation. [b] Distances (*r*) are in Å, angles (∠) in degrees. See text for parameter definitions and Figure 1(a) for atom numbering. The figures in parentheses are the estimated standard deviations of the last digits. [c] X is a dummy atom lying half-way between H(2) and H(3). [d] See text for description of this parameter.

Table 4. Refined ($r_{a3,1}$) and Calculated (r_e) Geometric Parameters for $Me_2HN{\cdot}BH_3$, **2**, from the GED Study.[a,b]

	param	$r_{a3,1}$	r_e	restraint
Independent				
p_1	rC–H mean	1.080(2)	1.084	—
p_2	rN–H	1.023(9)	1.014	0.01
p_3	rB–H mean	1.216(7)	1.206	0.01
p_4	rC–N	1.467(2)	1.467	—
p_5	rN–B	1.615(4)	1.619	—
p_6	∠B–N–C	111.9(2)	111.5	—
p_7	∠N–C–H average	110.6(3)	109.1	—
p_8	∠N–C–H difference 1	2.7(5)	2.8	0.5
p_9	∠N–C–H difference 2	1.0(5)	1.2	0.5
p_{10}	∠H–C–H average	109.8(9)	109.6	1.0
p_{11}	∠H–C–H difference	1.4(5)	1.4	0.5
p_{12}	∠N–B–H average	105.8(9)	105.2	—
p_{13}	∠N–B–H difference	0.7(5)	0.9	0.5
p_{14}	∠H–B–H	113.5(10)	113.4	1.0
p_{15}	∠H–N–C	107.2(5)	108.2	1.0
p_{16}	∠H–N–B	105.8(9)	106.1	1.0
Dependent				
p_{17}	∠C–N–C	112.4(4)	111.0	—
p_{18}	∠N–C(7)–H(8)	112.2(4)	111.0	—
p_{19}	∠N–C(7)–H(9)	110.2(4)	108.8	—
p_{20}	∠N–C(7)–H(10)	109.2(4)	107.6	—
p_{21}	∠H(8)–C(7)–H(10)	110.5(10)	110.5	—
p_{22}	∠H(9)–C(7)–H(10)	109.1(10)	108.9	—
p_{23}	∠N–B–H(4)	106.2(9)	105.6	—
p_{24}	∠N–B–H(6)	105.5(10)	104.7	—

[a] Refers to an MP2(full)/aug-cc-pVQZ calculation. [b] Distances (r) are in Å, angles (∠) in degrees. See text for parameter definitions and Figure 1(b) for atom numbering. The figures in parentheses are the estimated standard deviations of the last digits.

On the basis of the calculations described above, a C_s-symmetric model was written to describe the geometry of $Me_2HN{\cdot}BH_3$, **2**. The atom numbering used in the descriptions of the parameters is shown in Figure 1(b), and the parameters are listed in Table 4.

Five distance parameters were required, namely rC–H, rN–H, rB–H, rC–N and rN–B ($p_{1–5}$). Ten angle parameters were also employed (some as averages of values and related differences). The methyl groups,

while related to each other through symmetry, were quite asymmetric, and were therefore described using an average of the three different N–C–H angles (p_7) and two difference parameters ($p_{8–9}$), which were defined as follows:

p_8 = N–C(7)–H(8) – [N–C(7)–H(9) + N–C(7)–H(10)]/2

p_9 = N–C(7)–H(9) – N–C(7)–H(10)

To describe further the asymmetry of the methyl groups, two different H–C–H angles were defined by their average and the difference between them ($p_{10–11}$):

p_{11} = H(8)–C(7)–H(10) – H(9)–C(7)–H(10)

As the symmetry plane bisects the borane group, only two hydrogens were explicitly defined using an average of the two N–B–H angles (p_{12}), the difference between them [N–B–H(4) minus N–B–H(6)] (p_{13}), and the angle H(4)–B–H(6) (p_{14}). Assuming that the amino hydrogen atom also lies on the symmetry plane, the final two parameters required to define the geometry of **2** are H–N–C and H–N–B ($p_{15–16}$).

For both **1** and **2**, all the independent geometric parameters were refined using a least-squares method, and restraints were applied, using the SARACEN method,[52] to parameters (mainly those involving hydrogen, which is often poorly defined) that could not otherwise be refined (Tables 3 and 4). The restraints were based on values calculated at the MP2(full)/aug-cc-pVQZ level, and the uncertainties were loosely derived with reference to the change in value of that parameter during the series of calculations performed. Additionally, groups of amplitudes of vibration were refined (see Tables S2 and S3 for lists of amplitudes of vibration for **1** and **2**, respectively).

In the case of **1**, a parameter was included to describe the proportion of the molecules that do not undergo dissociation. It was found that the lowest *R* factor was obtained for a proportion of 0.67. To estimate the uncertainty on this value, the *R* factor was recorded at a number of values either side of 0.67, R_G/R_G(min) was plotted against the proportion of **1** (Figure 2), and, with reference to Hamilton's tables,[53] a line was drawn at 1.016 representing the 95% confidence limit. This suggests that the fraction of molecules of **1** remaining intact under the conditions of the experiment was approximately 0.67±0.03. The study of **1** and its dissociation products gave GED data that were rather noisy, and the fairly crude attempt to fit three separate species to the data has resulted in larger-than-usual *R* factors (R_G = 0.110, R_D = 0.061). For this refinement, the radial-distribution curves are given in Figure 3, the molecular-scattering intensity curves in Figure S1.

No such problems of dissociation were experienced with the dimethylamine adduct **2**. The success of the refinement of the relevant parameters in this case can be assessed numerically by the final *R* factor, which was R_G = 0.027 (R_D = 0.021), and visually by the goodness of fit of the radial-distribution and difference curves as displayed in Figure 4, and the molecular-scattering intensity curves (Figure S2).

The least-squares correlation matrices for **1** and **2** are given in Tables S4 and S5, and coordinates for the final GED structures and for the calculated structure [MP2(full)/aug-cc-pVQZ] are in Tables S6 and S7 and Tables S8 and S9, respectively.

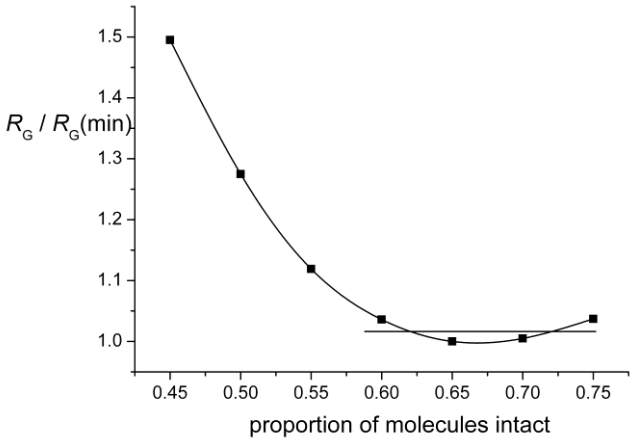

Figure 2. Plot of R_G/R_G(min) versus proportion of molecules of **1** that do not undergo dissociation. The horizontal line marks the 95% confidence limit.

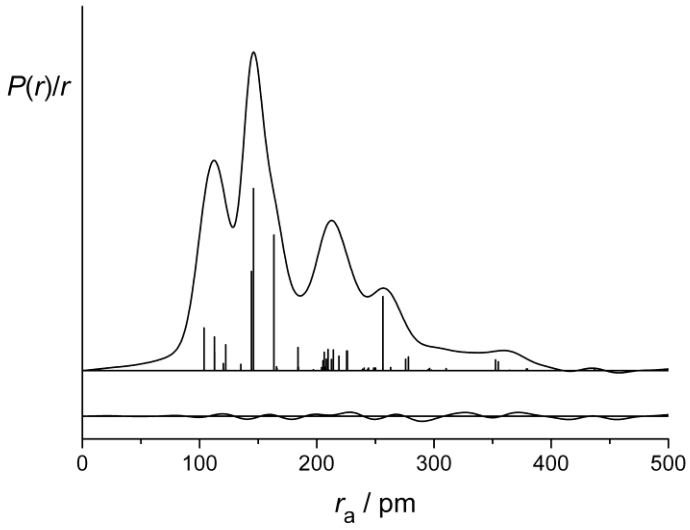

Figure 3. Experimental radial-distribution curves and theoretical-minus-experimental difference curves for $MeH_2N{\cdot}BH_3$, **1**, and its dissociation products. Before Fourier inversion the data were multiplied by $s{\cdot}\exp(-0.00002s^2)/(Z_C - f_C)(Z_N - f_N)$.

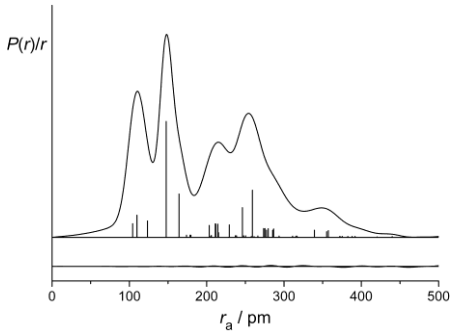

Figure 4. Experimental radial-distribution curves and theoretical-minus-experimental difference curves for $Me_2HN{\cdot}BH_3$, **2**. Before Fourier inversion the data were multiplied by $s{\cdot}\exp(-0.00002s^2)/(Z_C - f_C)(Z_N - f_N)$.

3.1(c) Comparisons of the structures of the isolated $Me_nH_{3-n}N{\cdot}BH_3$ molecules (n = 1–3)

Although GED[54,55] and microwave spectroscopic[56-58] studies have been carried out previously for $Me_3N{\cdot}BH_3$, microwave studies have been carried out for $H_3N{\cdot}BH_3$,[9] and considerable effort has been put into calculating the structures of all the members of the family $Me_nH_{3-n}N{\cdot}BH_3$ (n = 1–3),[21] the present studies afford the first experimental results regarding the structures of gaseous $MeH_2N{\cdot}BH_3$, **1**, and $Me_2HN{\cdot}BH_3$, **2**. Various distances determined by the different methods are listed in Table 5. Direct comparison is complicated by the fact that different distances (r_e from computational methods; r_a, r_g, r_{h1} and $r_{a3,1}$ from GED experiments; r_0 and r_s from microwave spectroscopic studies) have different physical meanings. This explains why, wherever possible, we have taken the literature values and estimated the chosen distances using calculated corrections.

Table 5. Comparison of Differently Defined B–N Distances for $Me_nH_{3-n}N{\cdot}BH_3$ (n = 1-3).[a]

adduct	r_a	r_g	r_{h1}	$r_{a3,1}$
$MeH_2N{\cdot}BH_3$	1.634(7)	1.637(7)	1.634(7)	1.602(7)
$Me_2HN{\cdot}BH_3$	1.644(4)	1.646(4)	1.642(4)	1.615(4)
$Me_3N{\cdot}BH_3$	1.653(2)	1.656(2)	1.652(2)	1.623(2)

[a] See text for details of how distances were calculated. All distances are in Å.

Our work has involved geometry optimizations to determine the structures of these molecules using a variety of computational methods and basis sets, as described in the Experimental section. Our conclusion is that some features of the structures are very dependent on the size of the basis sets used and also, but to a lesser degree, on the level of theory used. At the highest level and with the largest basis sets used [MP2(full)/aug-cc-

pVQZ], many of the calculated geometric parameters for $Me_2HN{\cdot}BH_3$ are close to those determined using GED ($r_{a3,1}$). This gives us some confidence in the results of our GED experiment.

The $r_{a3,1}$ values for the B–N distances determined for $MeH_2N{\cdot}BH_3$ [1.602(7) Å] and for $Me_2HN{\cdot}BH_3$ [1.615(4) Å] appear to be rather short when compared with the experimental value for the B–N distance obtained from the combined GED and MW study of gaseous $Me_3N{\cdot}BH_3$ (r_g = 1.656 ± 0.002 Å).[55] The origin of the short $r_{a3,1}$ values for **1** and **2** can be traced, however, to the corrections of 0.033 and 0.029 Å, respectively, that have been applied to the vibrationally averaged r_a values yielded by the GED experiments (Tables S2 and S3). Such corrections have been derived from anharmonic force fields calculated at the RHF/6-31G* level, as described earlier. To investigate this further, harmonic force fields (RHF/6-31G*) were used to generate corrections that, when applied to the r_a distance, yielded r_{h1} distances. For **1** and **2**, the corrections, k_{h1}, were 0.003 and 0.004 Å and, because $r_{h1} \approx r_a + u^2/r_a - k_{h1}$, the r_{h1} values for the B–N distances determined for **1** and **2** are estimated to be 1.634(7) and 1.642(4) Å, respectively. The B–N bonds are subject therefore to distinctly anharmonic vibrations, a factor not obvious from the vibrationally averaged r_a distance, or from the often-quoted r_{h1} and r_g distances. Moreover, the $r_{a3,1}$ values for **1** and **2** agree well with the results of high-level *ab initio* calculations [MP2(full)/aug-cc-pVQZ].

A search for previous studies of gaseous $Me_3N{\cdot}BH_3$ reveals that the structure was first studied in 1937 by GED,[54] then once in the 1960's,[56] twice in the 1970's[57,58] using microwave spectroscopy, and again in 1984 using a combination of new GED data with the rotation constants determined in the more recent microwave study.[55] Unsurprisingly, these studies report a range of B–N distances: 1.62±0.05 Å,[54] 1.65±0.02 Å,[56] 1.609 or 1.637 Å[57] (with the authors suggesting that the former is more believable), 1.638±0.01 Å,[58] and 1.656±0.002 Å.[55] In the present discussion, we will concentrate on the most recent GED data and the microwave study that yielded the rotation constants used with these data. The distance 1.656±0.002 Å is of the type r_g ($r_g \approx r_a + u^2/r_a$), and has been determined using a combination of GED data with microwave rotation constants.[55] Although the r_a value is not given, the amplitude of vibration, u, is known, and so an r_a value of 1.653 Å can be estimated. In the same way that we obtained corrections to find $r_{a3,1}$ distances for $Me_2HN{\cdot}BH_3$ and $MeH_2N{\cdot}BH_3$, we have used an anharmonic force field (RHF/6-31G*) and SHRINK to provide a correction for $Me_3N{\cdot}BH_3$. On this basis, we estimate $r_{a3,1}$B–N to be 1.623(2) Å, a value satisfyingly close to that determined by high-level *ab initio* calculations.

On the evidence of the quantum chemical calculations, the B–N distance (r_e) in amine-borane adducts of the type $Me_nH_{3-n}N{\cdot}BH_3$ varies but little with progressive methylation at the nitrogen center (spanning a total range not exceeding 0.006 Å), while $H_3N{\cdot}BH_3$ displays a distance about 0.02 Å longer than that in any of the methylamine-boranes. Refinement of the GED data for the methylamine-boranes under the SARACEN protocol[52] yields B–N distances (r_a, r_g, r_{hl}, *etc*.) that become slightly longer – by about 0.02 Å – as n increases from 1 to 3 (see Table 5). It should be appreciated, however, that partial dissociation causes the estimate for

$MeH_2N{\cdot}BH_3$ to be relatively poorly defined compared with those for $Me_2HN{\cdot}BH_3$ and $Me_3N{\cdot}BH_3$. As a test of this issue, the B–N distance in $MeH_2N{\cdot}BH_3$ was deliberately restrained to the calculated value of 1.624 Å, with a fairly tight uncertainty of ±0.005 Å. In fact, this had little effect on the refinement, raising the R_G factor by 0.02 and giving rise to negligible changes in the other parameters. We are bound to conclude therefore that the B–N distance is not a sensitive reporter on the coordinate link in this series of molecules. With no GED data to guide us, $H_3N{\cdot}BH_3$ cannot easily be compared with the methylamine-boranes, but the B–N distance determined from its microwave spectrum [r_s = 1.6576(16) Å][9] is consistent with the results of the present theoretical calculations in its implication that the B–N bond is indeed somewhat longer in this case. During the preparation of this manuscript, a further article on the structure of $H_3N{\cdot}BH_3$ appeared in the literature.[59] This paper, reporting the results of very high-level calculations using both MP2 and CCSD(T) theory, concludes that the equilibrium distance for B–N is 1.6455 Å. Furthermore, the authors use a calculated force field to obtain corrections that they then apply to the literature rotation constants for the molecule. As a result, they quote a semi-empirical B–N bond length of 1.6453 Å.

The combination of experiment and theory also shows that increasing charge transfer from N to B in the series $Me_nH_{3-n}N{\cdot}BH_3$ manifests itself in small changes (amounting to no more than 1-3°) in the N–B–H and B–N–C/B–N–H angles. Thus, the $Me_nH_{3-n}N$ unit becomes less pyramidal as BH_3 becomes more pyramidal with increasing n, as revealed for example in Table 2 listing the calculated sums of the angles subtended by the substituents at N (ΣN) and at B (ΣB). The barriers to rotation of the BH_3 group about the B–N bond have been calculated at the MP2(full)/6-311++G** level for each of the molecules in the series $Me_nH_{3-n}N{\cdot}BH_3$; they are 9.9, 11.8, 14.3, and 19.1 kJ mol^{-1} as n runs from 0 to 3. Progressing from $H_3N{\cdot}BH_3$ through the series to $Me_3N{\cdot}BH_3$ is attended by the following calculated energies (E_{diss}/E_{frag}) for dissociation in accordance with eq 1: 116.6/172.4, 138.3/197.2, 150.4/212.5, and 153.3/217.7 kJ mol^{-1} (where E_{frag} refers to dissociation into fragments frozen so as to retain the geometries they assume in the adduct). The E_{diss} values are in satisfactory agreement with experimental[19] and earlier theoretical[21] estimates, while the E_{frag} values imply that the total relaxation energies for the isolated dissociation fragments increase somewhat across the series, *viz*. from 55.8 to 64.4 kJ mol^{-1}.

3.2. The Crystal Structures of 1-3

Salient interatomic distances and interbond angles derived from the crystal structures determined by X-ray diffraction for single crystals of the adducts **1-3** are listed in Table 6. Before discussing these structures, however, we note that ammonia-borane, $H_3N{\cdot}BH_3$, forms monoclinic crystals in which the molecules pack in layers wherein a given molecule is surrounded by six others (see Figure 5i).[10,11] The most striking feature about the intermolecular contacts is the development of short N–H···H–B 'dihydrogen' bonds within the

layers with H···H distances measuring 1.97 and 2.19 Å (labeled 'B' in Figure 5i); between the layers (Figure 5ii) there is weaker binding that appears again to involve N–H···H–B interactions, now with H···H distances of 2.24 Å (labeled 'C') . Distances involving hydrogen atoms are calculated here and elsewhere in this section after 'normalization' of C–H, N–H, and B–H distances to typical neutron values (1.083, 1.009, and 1.190 Å, respectively).[47]

By contrast, methylamine-borane, $MeH_2N{\cdot}BH_3$, **1**, forms orthorhombic crystals in which the molecules of the adduct are linked in ribbons running along the *b* axis (Figure 6i). Within the ribbons successive molecules are aligned with the B–N bonds directed along the *c*-axis and antiparallel to one another; each pair of molecules is related by an inversion center and linked by two H···H contacts (labeled 'A') measuring 2.00 Å. The ribbons are in turn linked into a layer via H···H contacts ('B' in Figure 6ii) of 2.42 Å, and still weaker N–H···H–C interactions (at 2.89 Å, 'C') contribute to the forces holding the layers together.

The monoclinic crystals formed by dimethylamine-borane, $Me_2HN{\cdot}BH_3$, **2**, find the adduct molecules building up chains that run along the *b* axis (Figure 7i). Again H···H bonding is much in evidence in linking the molecules head-to-tail, this time featuring as a bifurcated $BH_2{\cdots}HN$ interaction with H···H distances of 1.95 and 2.08 Å (labeled 'B'). Each chain is surrounded by neighboring chains (Figure 7ii) experiencing relatively close interchain contacts ('A', 'D' and 'E'). The shortest H···H distances in each of these contacts and their inversion-related symmetry-equivalents are: H21···H33, 2.38 Å; H23···H11, 2.42 Å; and H32···H12, 2.55 Å.

Trimethylamine-borane, $Me_3N{\cdot}BH_3$, **3**, forms rhombohedral crystals in which the molecular coordination number of each molecule is 14, the structure being topologically similar to body-centered cubic packing. Head-to-tail interactions between the Me_3N and BH_3 groups link the molecules in chains along the *c* axis (Figure 8) with shortest C–H···H–B contacts of 2.66 Å.

Irrespective of the mode of aggregation, none of the methylamine-borane molecules suffers any radical change on crystallization. Due allowance must be made for the different estimates of interatomic distance (commonly amounting to about 0.1 Å for bonds in which hydrogen is engaged) made on the basis of electron or neutron diffraction on the one hand and of X-ray diffraction on the other. It then appears that the molecules invariably maintain a staggered conformation about the B–N bond, and that there is no significant change in the internal bond lengths of the amine and borane moieties on crystallization. In only two respects can a meaningful change be found between the intramolecular dimensions of the adduct molecules as they appear in the gaseous and crystalline phases. Firstly, with B–N distances of 1.594(2), 1.597(2), and 1.617(4) Å in crystalline **1**, **2**, and **3**, respectively, the coordinate link is observed consistently to contract (by 0.036-0.047 Å) with the switch from the gaseous to the solid phase. In this respect, the adducts follow the example of not only ammonia-borane,[10,11] but also other adducts featuring a coordinate link between a Group 13 acceptor and a

nitrogen base, *e.g.* $Me_3N{\cdot}GaH_3$.[60] Despite the energetic cost, compression of the polar coordinate link leads to an increased dipole moment for the adduct molecule, giving rise in turn to heightened Coulombic interactions, irrespective of any other factors governing the crystal packing. Simultaneously with the shortening of the B–N distance, the BH_3 pyramid acquires an even sharper pitch, with the sum of the three H–B–H angles decreasing by a further 3.3-6.2°. There appears also to be a corresponding tightening of the interbond angles at nitrogen (the sum decreasing by 2-3°) in the $Me_nH_{3-n}N$ fragment (see Table 6).

Table 6. Distances (Å) and Interbond Angles (deg) of the $Me_nH_{3-n}N{\cdot}BH_3$ Molecules (n = 1-3) in Crystalline **1**, **2**, and **3**, respectively

1	Distances[a]			
	B(1)–N(1)	1.5936(13)	B(1)–H(11)#1	1.134(9)
	N(1)–C(2)	1.4750(13)	B(1)–H(21)	1.121(13)
	N(1)–H(1)	0.881(9)	C(2)–H(12)	0.959(12)
	N(1)–H(1)#1	0.881(9)	C(2)–H(12)#1	0.959(12)
	B(1)–H(11)	1.134(9)	C(2)–H(22)	0.971(14)
	Angles[a]			
	B(1)–N(1)–C(2)	114.52(8)	N(1)–B(1)–H(21)	107.8(7)
	H(1)#1–N(1)–B(1)	109.5(6)	H(11)#1–B(1)–H(21)	111.6(6)
	H(1)#1–N(1)–C(2)	108.3(6)	H(11)–B(1)–H(21)	111.6(6)
	H(1)#1–N(1)–H(1)	106.2(12)	N(1)–C(2)–H(12)#1	108.0(6)
	B(1)–N(1)–H(1)	109.5(6)	N(1)–C(2)–H(12)	108.0(6)
	C(2)–N(1)–H(1)	108.3(6)	H(12)#1–C(2)–H(12)	111.0(14)
	N(1)–B(1)–H(11)#1	107.8(5)	N(1)–C(2)–H(22)	109.9(8)
	N(1)–B(1)–H(11)	107.8(5)	H(12)#1–C(2)–H(22)	109.9(8)
	H(11)#1–B(1)–H(11)	110.2(9)	H(12)–C(2)–H(22)	109.9(8)
2	Distances[a]			
	B(1)–N(1)	1.5965(13)	C(2)–H(12)	0.969(12)
	N(1)–C(2)	1.4734(13)	C(2)–H(22)	1.006(12)
	N(1)–C(3)	1.4731(14)	C(2)–H(32)	0.973(13)
	N(1)–H(1)	0.878(11)	C(3)–H(13)	0.989(12)
	B(1)–H(11)	1.118(6)	C(3)–H(23)	0.977(12)
	B(1)–H(21)	1.129(6)	C(3)–H(33)	0.982(12)
	B(1)–H(31)	1.125(6)		
	Angles[a]			
	B(1)–N(1)–C(2)	112.03(8)	N(1)–C(2)–H(12)	108.8(8)
	B(1)–N(1)–C(3)	112.71(8)	N(1)–C(2)–H(22)	106.9(7)
	C(2)–N(1)–C(3)	110.37(9)	H(12)–C(2)–H(22)	110.0(10)
	B(1)–N(1)–H(1)	107.0(7)	N(1)–C(2)–H(32)	108.7(8)
	C(2)–N(1)–H(1)	106.4(7)	H(12)–C(2)–H(32)	110.8(10)
	C(3)–N(1)–H(1)	108.0(7)	H(22)–C(2)–H(32)	111.4(10)
	N(1)–B(1)–H(11)	107.21(6)	N(1)–C(3)–H(13)	110.2(8)
	N(1)–B(1)–H(21)	107.21(6)	N(1)–C(3)–H(23)	108.4(8)
	H(11)–B(1)–H(21)	111.62(6)	H(13)–C(3)–H(23)	110.9(10)
	N(1)–B(1)–H(31)	107.23(6)	N(1)–C(3)–H(33)	108.1(8)
	H(11)–B(1)–H(31)	111.64(6)	H(13)–C(3)–H(33)	110.7(10)
	H(21)–B(1)–H(31)	111.63(6)	H(23)–C(3)–H(33)	108.5(10)

3	Distances[a]			
	B(1)#2–N(1)	1.617(4)	C(1)–H(21)	0.979(9)
	N(1)–C(1)	1.4825(16)	C(1)–H(21)#3	0.979(9)
	N(1)–C(1)#1	1.4832(16)	B(1)–H(1)	1.16(3)
	N(1)–C(1)#2	1.4832(16)	B(1)–H(1)#1	1.16(3)
	C(1)–H(11)	0.984(9)	B(1)–H(1)#2	1.16(3)
	Angles[a]			
	B(1)#2–N(1)–C(1)	110.53(9)	N(1)#4–C(1)–H(21)	109.3(10)
	B(1)#2–N(1)–C(1)#1	110.49(9)	N(1)–C(1)–H(21)	109.3(10)
	B(1)#2–N(1)–C(1)#2	110.46(9)	H(21)#3–C(1)–H(21)	105(2)
	C(1)#1–N(1)–C(1)#2	108.40(9)	H(11)–C(1)–H(21)	111.9(14)
	C(1)#1–N(1)–C(1)	108.44(9)	N(1)#4–B(1)–H(1)#1	106.4(20)
	C(1)#2–N(1)–C(1)	108.44(9)	N(1)#4–B(1)–H(1)#2	106.5(20)
	N(1)#4–C(1)–H(21)#3	109.3(10)	H(1)#1–B(1)–H(1)#2	112.3(17)
	N(1)–C(1)–H(21)#3	109.3(10)	N(1)#4–B(1)–H(1)	106.5(20)
	N(1)#4–C(1)–H(11)	109.3(16)	H(1)#1–B(1)–H(1)	112.3(17)
	N(1)–C(1)–H(11)	109.3(16)	H(1)#2–B(1)–H(1)	112.3(17)
	H(21)#3–C(1)–H(11)	111.9(14)		

[a] See Figures *x*-*x* + 2 for atom labeling.

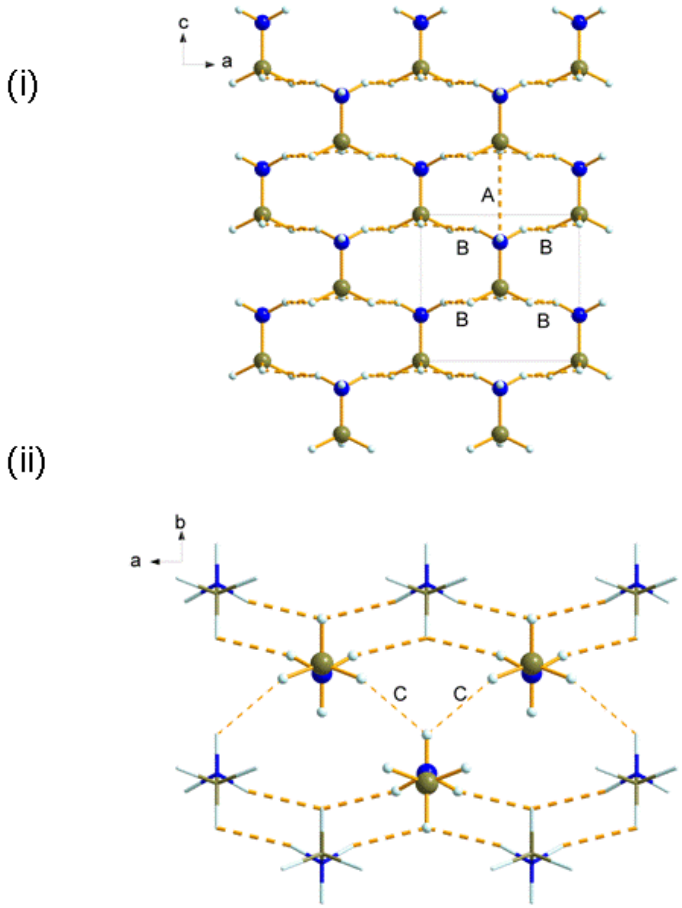

Figure 5. (i) Layers formed through H···H contacts in $H_3N{\cdot}BH_3$. The molecules lie on *m*.. sites. The labels A and B refer to the intermolecular contacts listed as A_0 and B_0 in Table 8. (ii) The crystal structure of $H_3N{\cdot}BH_3$

viewed along **c**. Only H···H contacts less than 2 Å are shown in order to emphasize the layers. The highlighted molecule in the lower layer makes contacts (C_0 in Table 8) to the highlighted molecules in the layer above. Color scheme: N blue, H white, B brown.

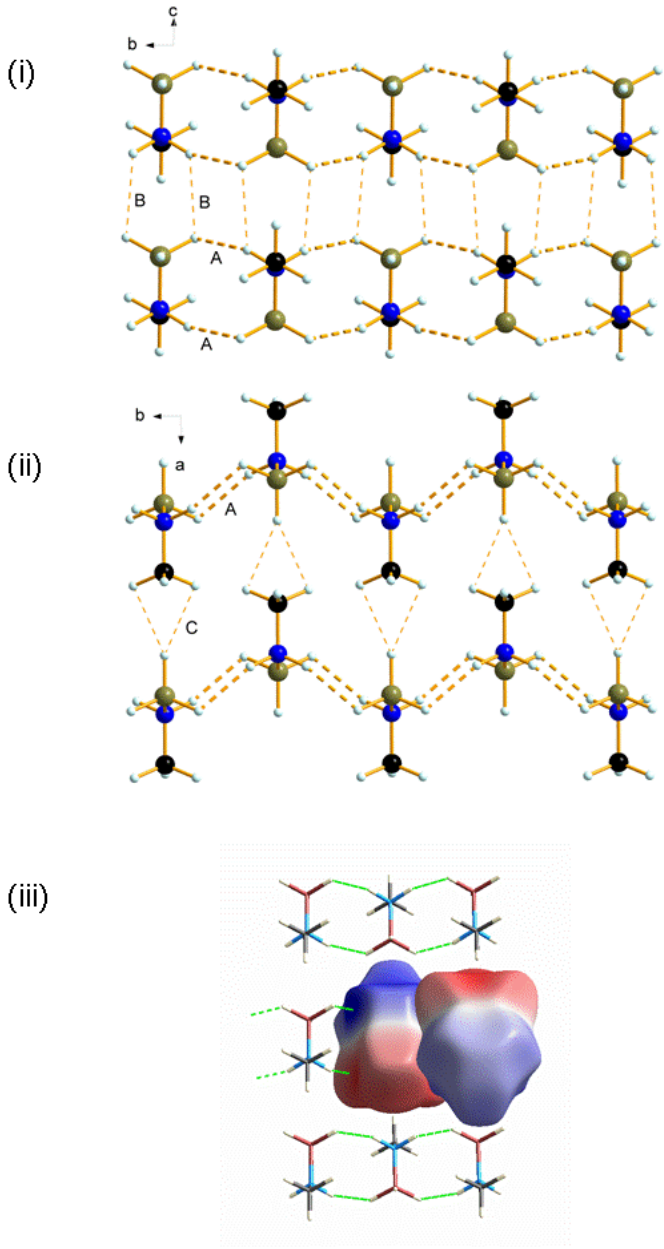

Figure 6. Formation of layers in the crystal structure of $MeH_2N{\cdot}BH_3$ (**1**) as viewed (i) along **a**, and (ii) along **c**. The labels A-C refer to the intermolecular contacts A_1-C_1 listed in Table 8. (iii) Packing in the layers in $MeH_2N{\cdot}BH_3$ with some molecules shown with Hirshfeld surfaces encoded with the electrostatic potential mapped over the range –0.1 au (red) to +0.1 au (blue). The same range is used in Figures 7-8 and in the *Table of Contents* figure.

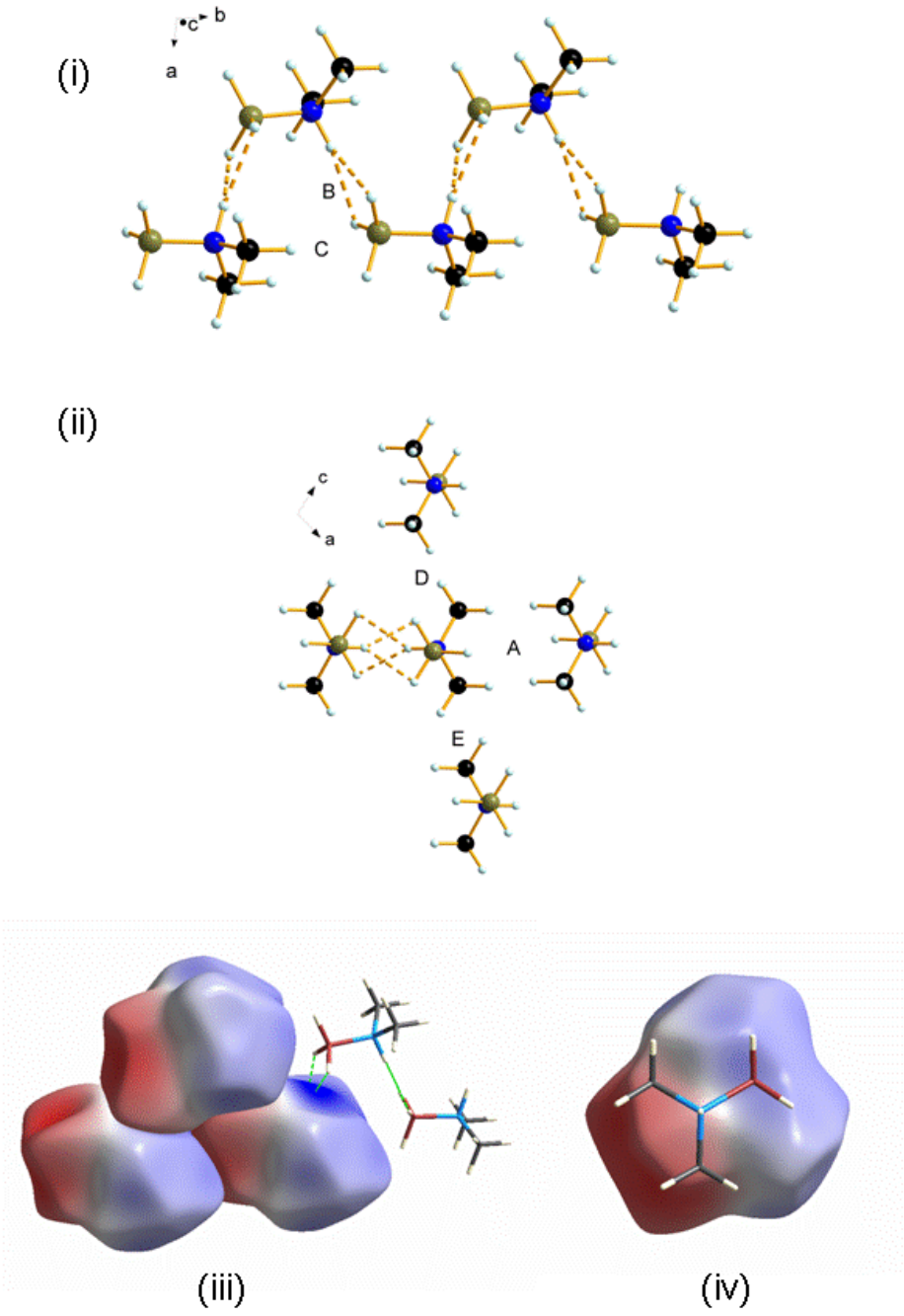

Figure 7. (i) Chains formed by H···H (contact B_2 in Table 8) and electrostatic interactions (C_2) in the crystal structure of $Me_2HN{\cdot}BH_3$ (**2**). (ii) The most significant inter-chain interactions (A_2, D_2 and E_2 in Table 8). (iii) Chains shown in (i) with the molecules having Hirshfeld surfaces encoded with the electrostatic potential; note the close disposition of the positive (blue) and negative (red) regions. (iv) The Coulombic term in interchain interaction A_3 illustrated using ESP-encoded Hirshfeld surfaces. Only one contacting surface is shown, the other being generated by an inversion center between the molecules.

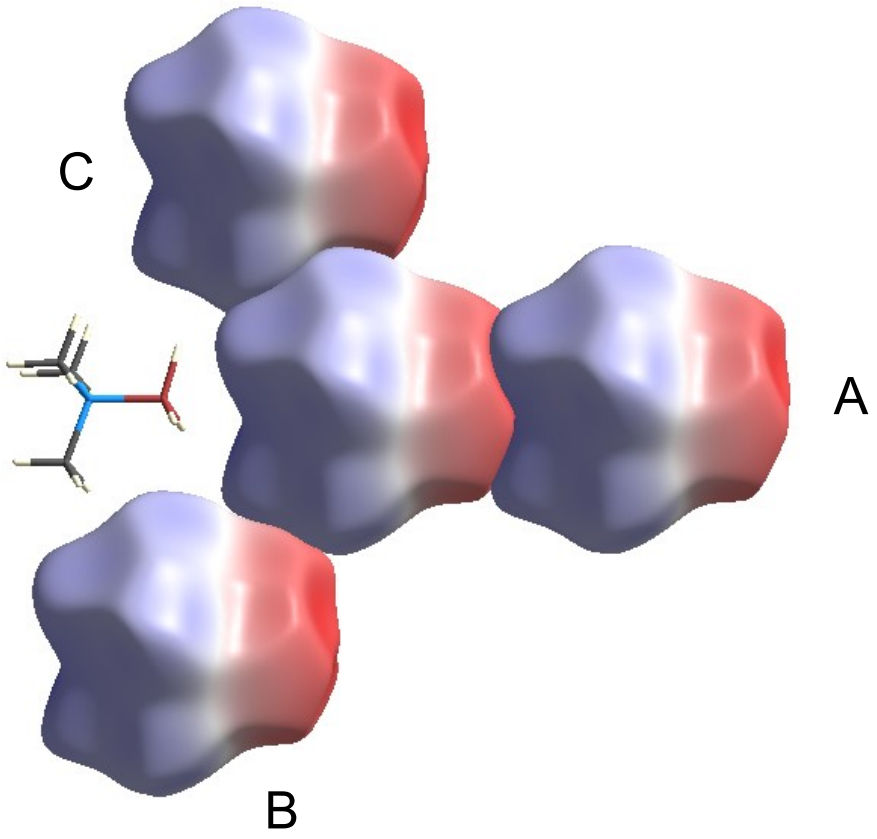

Figure 8 A head-to-tail arrangement of molecules in crystalline $Me_3N{\cdot}BH_3$ (**3**) forms chains running along the *c*-direction (here horizontal). This is interaction A_3 in Table 8. Neighboring chains interact through contacts B_3 and C_3, the latter being weaker. The molecules are shown with Hirshfeld surfaces encoded with the electrostatic potential; notice the larger blue-blue contact in interactions of type C.

3.3. Analysis of the Intermolecular Interactions in the Crystals: Results of Semi-Classical Density Sums (SCDS-PIXEL) Calculations

As a test of the reliability of our SCDS-PIXEL calculations, we begin by comparing the total lattice energy calculated for each of the crystalline adducts $Me_nH_{3-n}N{\cdot}BH_3$ (n = 0-3) with values from other sources,[15,61] including, particularly, experimental estimates of the sublimation energy.[22c] The calculations have also been extended to the six other boron-containing compounds noted earlier.

Table 7. Comparison of Total Lattice Energies, E_{TOTAL}, Calculated by SCDS-PIXEL Methods for the Crystalline Adducts $Me_nH_{3-n}N{\cdot}BH_3$ with the Experimental Sublimation Enthalpies, $\Delta_{sub}H_m$, and Earlier Theoretical Estimates[a]

adduct	E_{TOTAL}[b]	$\Delta_{sub}H_m$(exp)	other estimates
$H_3N{\cdot}BH_3$	–101.0	–97.0[c]	E_{TOTAL} = –79.2[d] $\Delta_{sub}H^o$ = –88.0[c]
$MeH_2N{\cdot}BH_3$	–93.3	–78.7(42)[e]	
$Me_2HN{\cdot}BH_3$	–85.0	–77.4(29)[e]	
$Me_3N{\cdot}BH_3$	–65.0	–56.9(8)[e]	

[a] All energies are in kJ mol^{-1}. [b] This work. [c] See reference 51. [d] Result of plane-wave density functional theory calculations, see reference 15. [e] See reference 22c.

The results are depicted in Figure 9, with more detailed information on the adducts set out in Table 7. While the PIXEL procedure tends to *over*estimate lattice energies of boron compounds on average by about 10%, for $H_3N{\cdot}BH_3$ they improve on earlier theoretical calculations involving plane-wave density functional theory[15] or other methods.[61] Amongst the adducts, the largest discrepancy is found in the case of $MeH_2N{\cdot}BH_3$, **1**.[22c] This may reflect weaknesses in the SCDS-PIXEL approach: sources of error are (a) the assumption that electron density distributions are undistorted in the solid state, (b) the assumed corrections from X-ray to neutron bond distances involving hydrogen, and (c) the neglect of zero-point energy and thermal corrections (d) neglect of intramolecular conformational changes which occur on sublimation. However, the reliability of the experimental value is also open to doubt, particularly as the vapor pressure plot for **1** shows a significantly greater degree of scatter in this case,[22b] and the vapor pressure equation derived may well give undue weight to a single, isolated point at low temperature (*ca*. 280 K). Still more doubt is raised by the findings of our GED experiments, which indicate that the vapor of **1** at *ca*. 360 K, unlike that of **2**, witnesses a significant degree of dissociation of the $MeH_2N{\cdot}BH_3$ molecules (see Section 3.1). We cannot be sure of course, but experiment, in the shape of the earlier vapor pressure measurements, may err at least as grossly as theory. Indeed, different *experimental* determinations of sublimation enthalpies can differ substantially even in the cases of well-behaved compounds: for example, the values quoted in ref 22c for BPh_3 are 103.8±2.5, 92.1±2.5, and 81.6±2.1 kJ mol^{-1}.

While there is a systematic error in the absolute values of the PIXEL lattice energies, the correlation coefficient between the data shown in Figure 9 is 0.95, meaning that the PIXEL method calculates *trends* in intermolecular energies very accurately. We feel therefore that this initial test justifies our proceeding to use the results of the calculations to analyze the details and energetics of molecular packing in crystals of the

$Me_nH_{3-n}N{\cdot}BH_3$ adducts. The energy values quoted below are likely to be upper limits, numerically too large by perhaps 10%.

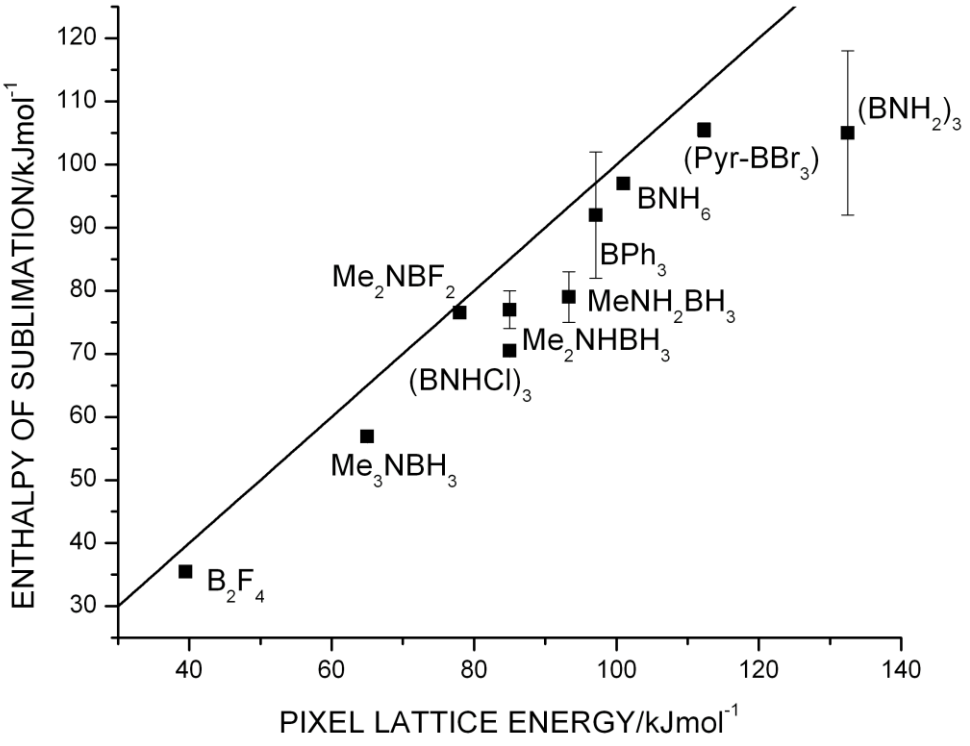

Figure 9. Comparison of experimental enthalpies of sublimation with total lattice energies calculated using the PIXEL procedure for a variety of boron-containing compounds. The line represents the function $y = x$; error bars are drawn where experimental estimates of precision are available.

$H_3N{\cdot}BH_3$. The three most significant contacts, $\mathbf{A_0}$-$\mathbf{C_0}$, are listed in Table 8; in addition, there are 14 contacts with energies between –5 and +14 kJ mol^{-1} that are long-range attractive and repulsive Coulombic interactions. Interactions $\mathbf{A_0}$ and $\mathbf{B_0}$ occur within the layers in which the molecules pack (Figure 5i). Intermolecular interaction $\mathbf{B_0}$ features dihydrogen bonds. While the energies of 'conventional' hydrogen bonds are usually dominated by the electrostatic term, the same is not true here, and both polarization and dispersion are important. The layers interact with layers above and below *via* weaker contacts $\mathbf{C_0}$ (Figure 5ii). The shortest H···H distances formed between the layers are only slightly longer than some of those within the layers, but the difference in energies is quite marked (19 *vs*. 5 kJ mol^{-1}).

Table 8. Intermolecular Interaction Energies (kJ mol^{-1}) Derived from SCDS-PIXEL Calculations for $H_3N.BH_3$, $MeH_2N.BH_3$, $Me_2HN.BH_3$, and $Me_3N.BH_3$ [a] On the basis of the data presented in Figure 9 the numerical values are likely to be slight overestimates.

adduct	interaction	Coulombic	polarization	dispersion	repulsion	TOTAL	Notes
$H_3N{\cdot}BH_3$	$\mathbf{A_0}$	–28.6	–4.9	–7.9	+6.0	–35.4	Intralayer head-to-tail Coulombic
	$\mathbf{B_0}$	–12.3	–16.1	–12.3	+22.1	–18.6	4 Intralayer contacts H···H 1.97 Å H···H 2.19 Å
	$\mathbf{C_0}$	–0.4	–4.3	–5.4	+5.1	–5.0	4 Interlayer contacts H···H 2.24 Å
$MeH_2N{\cdot}BH_3$ (**1**)	$\mathbf{A_1}$	–62.2	–24.3	–22.2	+37.9	–70.7	Ribbon forming H···H 2.00 Å
	$\mathbf{B_1}$	–26.7	–6.9	–12.7	+12.8	–33.5	Links ribbons into a layer H···H 2.42 Å
	$\mathbf{C_1}$	–7.4	–1.2	–3.2	+1.3	–10.5	Links the layers C–H···H–B 2.89 Å
$Me_2HN{\cdot}BH_3$ (**2**)	$\mathbf{A_2}$	–19.4	–3.9	–11.6	+8.7	–26.2	Interchain interaction
	$\mathbf{B_2}$	–22.0	–18.8	–17.5	+33.8	–24.5	Chain forming H···H = 1.95 and 2.08 Å
	$\mathbf{C_2}$	–18.5	–4.1	–9.5	+8.8	–23.4	Next-nearest neighbor interactions with chain
	$\mathbf{D_2}$	–16.8	–3.2	–8.3	+8.0	–20.3	Interchain interaction
	$\mathbf{E_2}$	–4.1	–0.9	–3.8	+1.5	–7.3	Interchain interaction
$Me_3N{\cdot}BH_3$ (**3**)	$\mathbf{A_3}$	–17.5	–4.8	–13.2	+11.4	–24.2	Head-to-tail chains C–H···H–B = 2.66 Å
	$\mathbf{B_3}$	–1.9	–1.2	–4.7	+2.4	–5.4	6 contacts in z = –2/3 and +2/3 layers
	$\mathbf{C_3}$	+4.0	–2.0	–10.8	+5.9	–2.9	6 contacts in z = –1/3 and +1/3 layers

[a] H···H distances calculated with normalized H-atom positions.

Some insight into the packing can be gained from a Hirshfeld surface plot colored to show the electrostatic potential, as recently described by McKinnon *et al*.[62] $H_3N{\cdot}BH_3$ is essentially a cylindrical molecule with positively and negatively charged ends. The pseudo- body-centered cubic packing established by contacts $\mathbf{B_0}$-$\mathbf{E_0}$ is readily understood in terms of optimization of contacts between positive and negative ends of the molecules [see *Table of Contents Figure*].

$MeH_2N{\cdot}BH_3$, 1. Again, there are three principal types of intermolecular contact, $\mathbf{A_1}$-$\mathbf{C_1}$, with the calculated energies listed in Table 8. Interaction $\mathbf{A_1}$ involves a pair of molecules, related by an inversion center, linked by two H···H contacts (at 2.00 Å, see Figure 6i). Successive inversion centers link the molecules into the ribbon running along the *b* axis. This contact is very strong – much stronger than any contact in $H_3N{\cdot}BH_3$; it incorporates two H···H bonds and anti-aligns the dipoles of the molecules. Contact $\mathbf{B_1}$ links the ribbons into a layer in the *bc* plane. The shortest H···H distance between the molecules involved in this contact is 2.42 Å; the interaction is rather similar to contact $\mathbf{A_0}$ in $H_3N{\cdot}BH_3$ (where the shortest H···H distance is 2.56 Å), except that the dispersion component is bigger. Interaction $\mathbf{C_1}$ links the layers. Now the shortest H···H contact, measuring 2.89 Å, is formed between a methyl H atom and an H atom of a BH_3 group (Figure 6ii). The energy is quite modest, and mostly electrostatic in origin. The interlayer stacking appears to be mediated by methyl groups and the interactions are therefore quite weak. This feature can also be illustrated by inspection of a Hirshfeld plot of electrostatic potential [Figure 6(iii)]; all the most 'electrostatically active' (*i.e*. most intensely colored) parts of the surface are oriented within the layers.

In addition to the contacts listed in Table 8, there are numerous longer range Coulombic interactions. These are both attractive and repulsive, and span the energy range from –8 to +8 kJ mol^{-1}.

$Me_2HN{\cdot}BH_3$, 2. Of the main intermolecular contacts in crystalline **2** listed in Table 8, four ($\mathbf{A_2}$-$\mathbf{D_2}$) have energies between –20 and –30 kJ mol^{-1}, while the fifth ($\mathbf{E_2}$) has a substantially lower energy at –7.3 kJ mol^{-1}; the energy of the next strongest contact is –3.9 kJ mol^{-1}. Interactions $\mathbf{B_2}$ and $\mathbf{C_2}$ build up the chain running along the *b* axis (Figure 7i). $\mathbf{B_2}$ comprises the two H···H contacts measuring 1.95 and 2.08 Å and in which the dispersion and polarization components are almost as energetic as the Coulombic term. Next-nearest neighbors in the chain are related by lattice translations along **b**, and take the form of head-to-tail arrangement of $Me_2HN{\cdot}BH_3$ molecules with an electrostatic interaction between successive amine and borane groups. The electrostatic potential plotted in Figure 7(iii) shows this clearly.

Each chain is surrounded by six neighboring chains, the four most energetic interactions being shown in Figure 7(ii). One of the interchain contacts ($\mathbf{A_2}$) is the strongest intermolecular interaction in the crystal, being a mixture of Coulombic and dispersion terms. The Coulombic part arises from contacts between the positively charged methyl H and the negatively charged borane H atoms [Figure 7(iv)]. Similar comments apply to

interactions $\mathbf{D_2}$ and $\mathbf{E_2}$, but the contact surface area is smaller, and this may explain why they are weaker contacts.

$Me_3N{\cdot}BH_3$, 3. The most significant intermolecular contacts in crystalline $Me_3N{\cdot}BH_3$ number three ($\mathbf{A_3}$-$\mathbf{C_3}$); their properties are as listed in Table 8. $\mathbf{A_3}$ involves two contacts, while $\mathbf{B_3}$ and $\mathbf{C_3}$ involve six contacts each. The **A**-type contacts are formed through head-to-tail interactions between the amine and borane groups, giving rise to the chain along the *c* axis (Figure 8). The 12 contacts corresponding to interactions $\mathbf{B_3}$ and $\mathbf{C_3}$ surround the chains along this axis, with energies dominated by dispersion terms. Interaction $\mathbf{C_3}$ is actually slightly repulsive in its Coulombic term, a feature that is understandable in the contacts between the blue regions of the middle and top surfaces of electrostatic potential shown in Figure 8.

Dihydrogen bond energies. The energies of the major N–H···H–B interactions that might reasonably be regarded as incorporating dihydrogen bonds in the adducts $Me_nH_{3-n}N{\cdot}BH_3$ are listed in Table 9. The PIXEL calculations evaluate molecule-molecule interaction energies. Single, strong H···H interactions are a feature of the crystal structures of both $H_3N{\cdot}BH_3$ and $MeH_2N{\cdot}BH_3$. The shortest H···H contacts in crystalline $MeH_2N{\cdot}BH_3$**,** linking the molecules in pairs, are noteworthy for the very strong electrostatic contribution involved. By contrast, the shortest H···H contact in crystalline $Me_2HN{\cdot}BH_3$ relates to a bifurcated dihydrogen bond, and is therefore rather different from the others. Perhaps the most nearly comparable H···H contacts are those in $H_3N{\cdot}BH_3$ and $MeH_2N{\cdot}BH_3$. The latter gives a stronger dihydrogen bond, with a larger electrostatic term. Consideration of the inductive effect of the methyl group might have been expected to lead to a *smaller* term, the *ab initio* population analysis placing charges of +0.37e and +0.26e on the amine H atoms in $H_3N{\cdot}BH_3$ and $MeH_2N{\cdot}BH_3$, respectively. The explanation for this apparent anomaly is not obvious, although it should be appreciated that there is more to each of the interactions than just the dihydrogen bonds. For example, the very strong interaction in $MeH_2N{\cdot}BH_3$ features a closely, anti-aligned pair of very polar molecules linked by two H···H contacts.

Finally, Table 10 lists for comparison the intermolecular contact energies mediated by dihydrogen bonds in $H_3N{\cdot}BH_3$ and $MeH_2N{\cdot}BH_3$ with those of some representative 'conventional' hydrogen bonds. On this evidence, dihydrogen bonds have polarization and dispersion energies that are similar to those in conventional hydrogen bonds, but smaller Coulombic energies. The greater relative importance of the polarization and dispersion terms appears therefore to distinguish dihydrogen from more conventional hydrogen bonds. Overall, however, the intermolecular interaction energies evaluated here are comparable with those of medium strength hydrogen bonds, such as those in phenol.

Table 9. Dihydrogen Bond Energies (kJ mol^{-1}) Estimated for $H_3N{\cdot}BH_3$, $MeH_2N{\cdot}BH_3$, and $Me_2HN{\cdot}BH_3$ on the Basis of SCDS-PIXEL Calculations [a]

adduct	E_{TOTAL}	H···H distance (Å)	contact	notes[b]
$H_3N{\cdot}BH_3$	–18.6 –5.0	1.97, 2.19 2.24	**B_0** **C_0**	Breakdown: E_C = –12.3 E_P = –16.1 E_D = –12.3 E_R = +22.1
$MeH_2N{\cdot}BH_3$	–70.7	2.00	**A_1**	Breakdown: E_C = –62.2 E_P = –24.3 E_D = –22.2 E_R = +37.9
$Me_2HN{\cdot}BH_3$	–24.5	1.95, 2.08	**B_2**	Breakdown: E_C = –22.0 E_P = –18.8 E_D = –17.5 E_R = +33.8

[a] H···H distances calculated with normalized H-atom positions. [b] Subscript abbreviations: C = Coulombic, P = polarization, D = dispersion, and R = repulsion.

Table 10. Comparison of Energy Terms (kJ mol^{-1}) in Dihydrogen and in some Representative Conventional Hydrogen Bonds [a]

interaction	type	E_C	E_P	E_D	E_R	E_{TOTAL}
Benzoic acid dimer[b]	O–H···O=C	–43	–17	–8	+33	–36
Benzamide dimer[b]	N–H···O=C	–38	–16	–10	+40	–23
Phenol dimer[b]	O–H···O–H	–41	–18	–14	+50	–22
$H_3N{\cdot}BH_3$[c]	N–H···H–B	–12	–16	–12	+22	–19

[a] Subscript abbreviations: C = Coulombic, P = polarization, D = dispersion, and R = repulsion. [b] See reference 25b. [c] This work.

4. Conclusions

In an effort to gain the fullest possible understanding of the structural properties of borane adducts of the type $Me_nH_{3-n}N{\cdot}BH_3$ for n = 0-3 in the gaseous and crystalline phases, we have determined the structures of the molecules $MeH_2N{\cdot}BH_3$, **1**, and $Me_2HN{\cdot}BH_3$, **2**, by gas-phase electron diffraction (GED), with restraints supplied by appropriate quantum chemical calculations. In addition, we have employed X-ray diffraction to determine the crystal structures of **1**, **2**, and $Me_3N{\cdot}BH_3$, **3**. The GED studies of **1** were complicated by partial dissociation of the adduct into MeH_2N and B_2H_6, but structures consistent with the results of high-level *ab initio* calculations have now been determined for all the gaseous molecules in this series. Despite a 23% increase in the experimentally estimated dissociation energy on passing from $H_3N{\cdot}BH_3$ to $Me_3N{\cdot}BH_3$, the geometries of the adduct molecules reveal only slight changes with progressive methylation at the nitrogen center. Thus, the B–N bond length varies but little for the methylamine-boranes, while increasing slightly (by about 0.02 Å) in $H_3N{\cdot}BH_3$. There are also minor changes in the angles subtended by the bonds to the substituents at the B and N centers, with the $C_nH_{3-n}N$ moiety tending to become slightly less pyramidal and the BH_3 one slightly more pyramidal as n increases.

The crystallographic studies show that all the adducts form crystals in which the $Me_nH_{3-n}N{\cdot}BH_3$ molecules do not deviate greatly from the structures they assume in the gas phase. Crystallization causes a shortening of the B–N link by about 0.094 Å for $H_3N{\cdot}BH_3$ [9-11] and 0.036-0.047 Å for the methylamine-boranes, while there is also some tightening of the interbond angles made by the substituents at B and N. Where $H_3N{\cdot}BH_3$ has already been shown to form crystals in which the adduct molecules pack in layers, the methylamine-boranes, **1**-**3**, all form crystals in which the molecules are linked in chains. In common with $H_3N{\cdot}BH_3$, both $MeH_2N{\cdot}BH_3$ and $Me_2HN{\cdot}BH_3$ reveal evidence of significant intermolecular N–H···H–B 'dihydrogen' bonds with short H···H contacts measuring about 2.0 Å. The relative importance of these and other secondary interactions has been assessed for all the members of the series by carrying out Semi-Classical Density Sums (SCDS-PIXEL) calculations.[25] Hence we conclude that dihydrogen bonds resemble conventional hydrogen bonds in their polarization and dispersion energies, but differ from them in having distinctly smaller Coulombic energies. Nevertheless, the total intermolecular interaction energies evaluated for dihydrogen bonds in $H_3N{\cdot}BH_3$ and the methylamine-boranes are comparable overall with those of such conventional hydrogen bonds as are found, for example, in solid phenol.

Footnotes and References

[1] Stock, A. *Hydrides of Boron and Silicon*; Cornell University Press: Ithaca, NY, 1933; p 58.

[2] Geanangel, R. A.; Shore, S. G. *Prep. Inorg. React*. **1966**, *3*, 123.

[3] Wiberg, E.; Amberger, E. *Hydrides of the Elements of Main Groups I-IV*; Elsevier: Amsterdam, the Netherlands, 1971.

[4] *Gmelin Handbook of Inorganic Chemistry*, 8th edn., *Boron Compounds*, Syst. No. 13; Supplements 1-4; Springer-Verlag: Berlin, Germany, 1974-1991.

[5] Muetterties, E. L., Ed. *Boron Hydride Chemistry*; Academic Press: New York, 1975.

[6] *Supplement to Mellor's Comprehensive Treatise on Inorganic and Theoretical Chemistry*, Vol. V, *Boron*. Part BI: *Boron-Hydrogen Compounds*; Longman: London, U.K., 1980-1981.

[7] Lane, C. F. *N-B-H Survey*; Contract # DE-FC36-05GO15060; Northern Arizona University, 2006.

[8] Stephens, F. H.; Pons, V.; Baker, R. T. *Dalton Trans*. **2007**, 2613.

[9] Suenram, R. D.; Thorne, L. R. *Chem. Phys. Lett*. **1981**, *78*, 157. Thorne, L. R.; Suenram, R. D.; Lovas, F. J. *J. Chem. Phys*. **1983**, *78*, 167.

[10] Bühl, M.; Steinke, T.; Schleyer, P. v. R.; Boese, R. *Angew. Chem., Int. Ed. Engl*. **1991**, *30*, 1160.

[11] Klooster, W. T.; Koetzle, T. F.; Siegbahn, P. E. M.; Richardson, T. B.; Crabtree, R. H. *J. Am. Chem. Soc*. **1999**, *121*, 6337.

[12] Crabtree, R. H.; Siegbahn, P. E. M.; Eisenstein, O.; Rheingold, A. L.; Koetzle, T. F. *Acc. Chem. Res*. **1996**, *29*, 348.

[13] See, for example: Trudel, S.; Gilson, D. F. R. *Inorg. Chem*. **2003**, *42*, 2814. Custelcean, R.; Dreger, Z. A. *J. Phys. Chem. B* **2003**, *107*, 9231.

[14] See, for example: Richardson, T. B.; de Gala, S.; Crabtree, R. H. *J. Am. Chem. Soc.* **1995**, *117*, 12875. Cramer, C. J.; Gladfelter, W. L. *Inorg. Chem*. **1997**, *36*, 5358. Popelier, P. L. A. *J. Phys. Chem. A* **1998**, *102*, 1873. Kulkarni, S. A. *J. Phys. Chem. A* **1998**, *102*, 7704. Li, J.; Zhao, F.; Jing, F. *J. Chem. Phys*. **2002**, *116*, 25. Merino, G.; Bakhmutov, V. I.; Vela, A. *J. Phys. Chem. A* **2002**, *106*, 8491. Meng, Y.; Zhou, Z.; Duan, C.; Wang, B.; Zhong, Q. *J. Mol. Struct.: THEOCHEM* **2005**, *713*, 135. Nguyen, V. S.; Matus, M. H.; Grant, D. J.; Nguyen, M. T.; Dixon, D. A. *J. Phys. Chem. A* **2007**, *111*, 8844. Alkorta, I.; Elguero, J.; Grabowski, S. J. *J. Phys. Chem. A* **2008**, *112*, 2721.

[15] Morrison, C. A.; Siddick, M. M. *Angew. Chem., Int. Ed*. **2004**, *43*, 4780.

[16] Beachley, O. T. *Inorg. Chem*. **1965**, *4*, 1823.

[17] Bauer, S. H. *J. Am. Chem. Soc*. **1937**, *59*, 1823. Iijima, K.; Adachi, N.; Shibata, S. *Bull. Chem. Soc. Jpn*. **1984**, *57*, 3269.

[18] Cassoux, P.; Kuczkowski, R. L.; Bryan, P. S.; Taylor, R. C. *Inorg. Chem*. **1975**, *14*, 126.

[19] See, for example: Haaland, A. *Angew. Chem., Int. Ed. Engl*. **1989**, *28*, 992 and references cited therein. Lias, S. G.; Bartmess, J. E.; Liebman, J. F.; Holmess, J. L.; Levin, R. D.; Mallard, W. G. *J. Phys. Chem. Ref. Data* **1988**, *17*, Suppl. 1.

[20] Smith, B. J.; Radom, L. *J. Phys. Chem*. **1995**, *99*, 6468.

[21] See, for example: Anane, H.; Jarid, A.; Boutalib, A.; Nebot-Gil, I.; Tomás, F. *J. Mol. Struct.: THEOCHEM* **1998**, *455*, 51.

[22] (a) Schlesinger, H. I.; Ritter, D. M.; Burg, A. B. *J. Am. Chem. Soc*. **1938**. *60*, 1296. (b) Alton, E. R.; Brown, R. D.; Carter, J. C.; Taylor, R. C. *J. Am. Chem. Soc*. **1959**, *81*, 3550. (c) Chickos, J. S.; Acree, W. E., Jr. *J. Phys. Chem. Ref. Data* **2002**, *31*, 634-5.

[23] Nöth, H.; Beyer, H. *Chem. Ber*. **1960**, *93*, 939.

[24] See, for example: Fakioğlu, E.; Yürüm, Y.; Nejat Veziroğlu, T. *Int. J. Hydrogen Energy* **2004**, *29*, 1371. Dixon, D. A.; Gutowski, M. *J. Phys. Chem. A* **2005**, *109*, 5129. Gutowska, A.; Li, L.; Shin, Y.; Wang, C. M.; Li, X. S.; Linehan, J. C.; Smith, R. S.; Kay, B. D.; Schmid, B.; Shaw, W.; Gutowski, M.; Autrey, T. *Angew. Chem., Int. Ed*. **2005**, *44*, 3578. Bluhm, M. E.; Bradley, M. G.; Butterick, R., III; Kusari, U.; Sneddon, L. G. *J. Am. Chem. Soc*. **2006**, *128*, 7748. Baitalow, F.; Wolf, G.; Grolier, J.-P. E.; Dan, F.; Randzio, S. L. *Thermochem. Acta* **2006**, *445*, 121. Cheng, F.; Ma, H.; Li, Y.; Chen, J. *Inorg. Chem*. **2007**, *46*, 788. Keaton, R. J.; Blacquiere, J. M.; Baker, R. T. *J. Am. Chem. Soc*. **2007**, *129*, 1844. Stephens, F. H.; Baker, R. T.; Matus, M. H.; Grant, D. J.; Dixon, D. A. *Angew. Chem., Int. Ed*. **2007**, *46*, 746. Stowe, A. C.; Shaw, W. J.; Linehan, J. C.; Schmid, B.; Autrey, T. *Phys. Chem. Chem. Phys*. **2007**, *9*, 1831. Mohajeri, N.; T-Raissi, A.; Adebiyi, O. *J. Power Sources* **2007**, *167*, 482. Nguyen, M. T.; Nguyen, V. S.; Matus, M. H.; Gopakumar, G.; Dixon, D. A. *J. Phys. Chem. A* **2007**, *111*, 679. Marder, T. B. *Angew. Chem., Int. Ed*. **2007**, *46*, 8116. Yan, J.-M.; Zhang, X.-B.; Han, S.; Shioyama, H.; Xu, Q. *Angew. Chem. Int. Ed*. **2008**, *47*, 2287.

[25] (a) Dunitz, J. D.; Gavezzotti, A. *Angew. Chem. Int. Ed*. **2005**, *44*, 1766. (b) Gavezzotti, A. *Molecular Aggregation: Structure Analysis and Molecular Simulation of Crystals and Liquids*; Oxford University Press: Oxford and New York, 2007.

[26] Schaeffer, G. W.; Anderson, E. R. *J. Am. Chem. Soc*. **1949**, *71*, 2143.

[27] Shriver, D. F.; Shirk, A. E. *Inorg. Synth*. **1977**, *17*, 42.

[28] Huntley, C. M.; Laurenson, G. S.; Rankin, D. W. H. *J. Chem. Soc., Dalton Trans*. **1980**, 954.

[29] Fleischer, H.; Wann, D. A.; Hinchley, S. L.; Borisenko, K. B.; Lewis, J. R.; Mawhorter, R. J.; Robertson, H. E.; Rankin, D. W. H. *Dalton Trans*. **2005**, 3221.

[30] Hinchley, S. L.; Robertson, H. E.; Borisenko, K. B.; Turner, A. R.; Johnston, B. F.; Rankin, D. W. H.; Ahmadian, M.; Jones, J. N.; Cowley, A. H. *Dalton Trans*. **2004**, 2469.

[31] Ross, A. W.; Fink, M.; Hilderbrandt, R. In *International Tables for Crystallography*; Wilson, A. J. C., Ed.; Kluwer Academic Publishers: Dordrecht, The Netherlands, 1992: Vol. 2, p 245.

[32] SIR 92: Altomare, A; Cascarano, G.; Giacovazzo, C.; Guagliardi, A. J. *J. Appl. Crystallogr*. **1993**, *26*, 343.

[33] CRYSTALS: Betteridge, P. W.; Carruthers, J. R.; Cooper, R. I.; Prout, K.; Watkin, D. J. *J. Appl. Crystallogr*. **2003**, *36*, 1487.

[34] DIAMOND: Brandenburg, K.; Putz, H. *DIAMOND*; Crystal Impact: Bonn, Germany, 2005.

[35] MERCURY: Macrae, C. F.; Bruno, I. J.; Chisholm, J. A.; Edgington, P. R.; McCabe, P.; Pidcock, E.; Rodriguez-Monge, L.; Taylor, R.; van de Streek, J.; Wood, P. A. *J. Appl. Crystallogr*. **2008**, *41*, 466.

[36] PLATON: Spek, A. L. *J. Appl. Crystallogr*. **2003**, *36*, 7.

[37] National Service for Computational Chemistry Software (NSCCS). URL http://www.nsccs.ac.uk

[38] EaStCHEM Research Computing Facility (http://www.eastchem.ac.uk/rcf). This facility is partially supported by the eDIKT initiative (http://www.edikt.org).

[39] Frisch, M. J.; Trucks, G. W.; Schlegel, H. B.; Scuseria, G. E.; Robb, M. A.; Cheeseman, J. R.; Montgomery, J. A., Jr.; Vreven, T.; Kudin, K. N.; Burant, J. C.; Millam, J. M.; Iyengar, S. S.; Tomasi, J.; Barone, V.; Mennucci, B.; Cossi, M.; Scalmani, G.; Rega, N.; Petersson, G. A.; Nakatsuji, H.; Hada, M.; Ehara, M.; Toyota, K.; Fukuda, R.; Hasegawa, J.; Ishida, M.; Nakajima, T.; Honda, Y.; Kitao, O.; Nakai, H.; Klene, M.; Li, X.; Knox, J. E.; Hratchian, H. P.; Cross, J. B.; Adamo, C.; Jaramillo, J.; Gomperts, R.; Stratmann, R. E.; Yazyev, O.; Austin, A. J.; Cammi, R.; Pomelli, C.; Ochterski, J. W.; Ayala, P. Y.; Morokuma, K.; Voth, G. A.; Salvador, P.; Dannenberg, J. J.; Zakrzewski, V. G.; Dapprich, S.; Daniels, A. D.; Strain, M. C.; Farkas, O.; Malick, D. K.; Rabuck, A. D.; Raghavachari, K.; Foresman, J. B.; Ortiz, J. V.; Cui, Q.; Baboul, A. G.; Clifford, S.; Cioslowski, J.; Stefanov, B. B.; Liu, G.; Liashenko, A.; Piskorz, P.; Komaromi, I.; Martin, R. L.; Fox, D. J.; Keith, T.; Al-Laham, M. A.; Peng, C. Y.; Nanayakkara, A.;

Challacombe, M.; Gill, P. M. W.; Johnson, B.; Chen, W.; Wong, M. W.; Gonzalez, C.; Pople, J. A. *Gaussian 03, Revision C.02*; Gaussian, Inc.: Wallingford, CT, 2004.

[40] Binkley, J. S.; Pople, J. A.; Hehre, W. J. *J. Am. Chem. Soc.* **1980**, *102*, 939. Gordon, M. S.; Binkley, J. S.; Pople, J. A.; Pietro, W. J.; Hehre, W. J. *J. Am. Chem. Soc.* **1982**, *104*, 2797. Pietro, W. J.; Francl, M. M.; Hehre, W. J.; DeFrees, D. J.; Pople, J. A.; Binkley, J. S. *J. Am. Chem. Soc.* **1982**, *104*, 5039.

[41] Hehre, W. J.; Ditchfield, R.; Pople, J. A. *J. Chem. Phys.* **1972**, *56*, 2257. Hariharan, P. C.; Pople, J. A. *Theor. Chim. Acta* **1973**, *28*, 213. Gordon, M. S. *Chem. Phys. Lett.* **1980**, *76*, 163.

[42] Møller, C.; Plesset, M. S. *Phys. Rev.* **1934**, *46*, 618.

[43] Krishnan, R.; Binkley, J. S.; Seeger R.; Pople, J. A. *J. Chem. Phys.* **1980**, *72*, 650. McLean, A. D.; Chandler, G. S. *J. Chem. Phys.* **1980**, *72*, 5639.

[44] Sipachev, V. A. *J. Mol. Struct.* (*THEOCHEM*) **1985**, *121*, 143. Sipachev, V. A. *J. Mol. Struct.* **2001**, *567*, 67.

[45] McCaffrey, P. D.; Mawhorter, R. J.; Turner, A. R.; Brain, P. T.; Rankin, D. W. H. *J. Phys. Chem. A* **2007**, *111*, 6103.

[46] (a) Gavezzotti, A. *OPiX*: a computer program package for the calculation of intermolecular interactions and crystal energies; University of Milan, Italy, 2003. (b) Gavezzotti, A. *Z. Kristallogr*. **2005**, *220*, 499.

[47] Desiraju, G.; Steiner, T. *The Weak Hydrogen Bond in Structural Chemistry and Biology*; Oxford University Press: Oxford and New York, 2001.

[48] Allen, F. H. *Acta Crystallogr., Sect. B: Struct. Sci*. **2002**, *B58*, 380.

[49] Wood, P. A.; Francis, D.; Marshall, W. G.; Moggach, S. A.; Parsons, S.; Pidcock, E.; Rohl, A. L. *CrystEngComm* **2008**, *10*, 1154.

[50] van Eijck, B. P.; Kroon, J. *J. Phys. Chem. B* **1997**, *101*, 1096.

[51] Wolff, S. K.; Grimwood, D. J.; McKinnon, J. J.; Jayatilaka, D.; Spackman, M. A. *Crystal_Explorer*, version 2.1(381), University of Western Australia, Australia, 2007.

[52] Blake, A. J.; Brain, P. T.; McNab, H.; Miller, J.; Morrison, C. A.; Parsons, S.; Rankin, D. W. H.; Robertson, H. E.; Smart, B. A. *J. Phys. Chem.* **1996**, *100*, 12280. Brain, P. T.; Morrison, C. A.; Parsons, S.; Rankin, D. W. H. *J. Chem. Soc., Dalton Trans.* **1996**, 4589. Mitzel, N. W.; Rankin, D. W. H. *Dalton Trans.* **2003**, 3650.

[53] Hamilton, W. C. *Acta Cryst.* **1965**, *18*, 502.

[54] Bauer, S. H. *J. Am. Chem. Soc.* **1937**, *59*, 1804.

[55] Iijima, K.; Adachi, N.; Shibata, S. *Bull. Chem. Soc. Jpn.* **1984**, *57*, 3269.

[56] Schirdewahn, H. G. *Ph.D. Thesis*, University of Freiburg, 1965.

[57] Durig, J. R.; Li, Y. S.; Odom, J. D. *J. Mol. Struct.* **1973**, *16*, 443.

[58] Cassoux, P.; Kuczkowski, R. L.; Bryan, P. S.; Taylor, R. C. *Inorg. Chem.* **1975**, *14*, 126.

[59] Demaison, J.; Liévin, J.; Császár, A. G.; Gutle, C. *J. Phys. Chem. A* **2008**, *112*, 4477.

[60] See, for example, the following: Brain, P. T.; Brown, H. E.; Downs, A. J.; Greene, T. M.; Johnsen, E.; Parsons, S.; Rankin, D. W. H.; Smart, B. A.; Tang, C. Y. *J. Chem. Soc., Dalton Trans*. **1998**, 3685. Marchant, S.; Tang, C. Y.; Downs, A. J.; Greene, T. M.; Himmel, H.-J.; Parsons, S. *Dalton Trans*. **2005**, 3281. Wann, D. A.; Blockhuys, F.; Van Alsenoy, C.; Robertson, H. E.; Himmel, H.-J.; Tang, C. Y.; Cowley, A. R.; Downs, A. J.; Rankin, D. W. H. *Dalton Trans*. **2007**, 1687.

[61] Matus, M. H.; Anderson, K. D.; Camaioni, D. M.; Autrey, S. T.; Dixon, D. A. *J. Phys. Chem. A* **2007**, *111*, 4411.

[62] Spackman, M. A.; McKinnon, J. J.; Jayatilaka, D. *CrystEngComm* **2008**, *10*, 377.